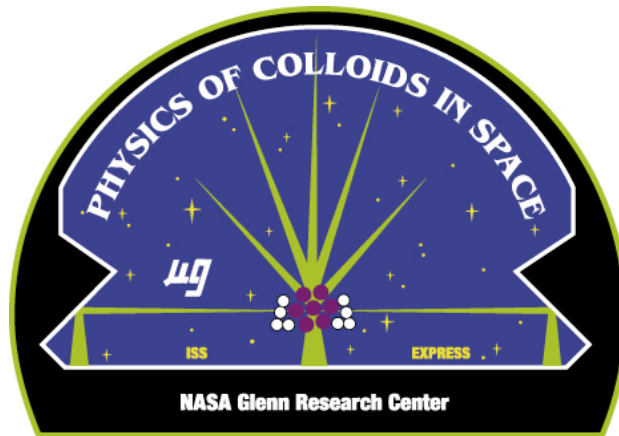


# FINAL REPORT

## Physics of Colloids in Space (PCS)

Submitted to  
NASA Glenn Research Center  
Cleveland, OH  
Grant NAG3-2284



**Principal Investigator:** Professor David A. Weitz  
Harvard University, Cambridge Massachusetts

**Co-Investigator:** Professor Peter N. Pusey  
University of Edinburgh, United Kingdom

**Project Scientist:** Dr. Subramanian Sankaran  
National Center for Space Exploration Research,  
Cleveland, Ohio

**Project Manager:** Michael P. Doherty  
NASA Glenn Research Center, Cleveland, Ohio.

August 2005



## **Physics of Colloids in Space**

### Final Report

The Physics of Colloids in Space project flew one experiment in the International Space Station during a period when the goal of the ISS was still to carry out high quality microgravity research.

The experiment was highly successful, and has resulted in four papers being submitted based exclusively on the results obtained in the experiment. Numerous other papers have been published based on the related ground-based experiments.

The PCS experiment consisted of eight sample cells. The papers discuss results obtained in five of them: two sample cells containing binary crystal alloy, two containing colloidal aggregates, and one containing a sample that undergoes spinodal decomposition.

The results from each of these experiments are discussed in the accompanying papers and a description of the apparatus is discussed in the paper at the end.

Further details on PCS, as well as related research, can be found at <http://www.deas.harvard.edu/projects/weitzlab>.



## Limits to Gelation in Colloidal Aggregation

S. Manley,<sup>1</sup> L. Cipelletti,<sup>1,\*</sup> V. Trappe,<sup>2</sup> A. E. Bailey,<sup>1,†</sup> R. J. Christianson,<sup>1</sup> U. Gasser,<sup>1,‡</sup> V. Prasad,<sup>1,§</sup> P. N. Segre,<sup>1,||</sup> M. P. Doherty,<sup>3</sup> S. Sankaran,<sup>3</sup> A. L. Jankovsky,<sup>3</sup> B. Shiley,<sup>3</sup> J. Bowen,<sup>4</sup> J. Eggers,<sup>4</sup> C. Kurta,<sup>4</sup> T. Lorik,<sup>4</sup> and D. A. Weitz<sup>1</sup>

<sup>1</sup>*Department of Physics & DEAS, Harvard University, Cambridge, Massachusetts 02138, USA*

<sup>2</sup>*Department of Physics, University of Fribourg, CH-1700 Fribourg, Switzerland*

<sup>3</sup>*NASA Glenn Research Center, Brook Park, Ohio 44135, USA*

<sup>4</sup>*Zin Technologies, Inc., Brook Park, Ohio 44142, USA*

(Received 22 March 2004; published 2 September 2004)

We show that the dynamics of large fractal colloid aggregates are well described by a combination of translational and rotational diffusion and internal elastic fluctuations, allowing both the aggregate size and internal elasticity to be determined by dynamic light scattering. The comparison of results obtained in microgravity and on Earth demonstrates that cluster growth is limited by gravity-induced restructuring. In the absence of gravity, thermal fluctuations ultimately inhibit fractal growth and set the fundamental limitation to the lowest volume fraction which will gel.

DOI: 10.1103/PhysRevLett.93.108302

PACS numbers: 82.70.Gg, 61.43.Hv, 62.20.Dc, 82.70.Dd

Diffusion-limited cluster aggregation (DLCA) of colloidal particles results in the formation of tenuous, highly disordered clusters; nevertheless, their fractal nature leads to a well determined scale-invariant symmetry, which facilitates our understanding of the structure and growth kinetics of such aggregates. Growth by DLCA is predicted to result in a power-law increase in cluster size with time,  $R_c \sim t^{1/d_f}$ , where  $R_c$  is the average cluster radius and  $d_f$  is the fractal dimension [1]. This growth proceeds until the clusters span space, whereupon the system gels; this occurs when  $R_c = a\phi_0^{1/(d_f-3)}$ , where  $a$  is the colloid radius and  $\phi_0$  is the initial particle volume fraction [2,3]. Since the density of fractal objects decreases as their size increases, colloidal aggregates can, in principle, gel to form an elastic solid at arbitrarily low volume fractions. However, a solid in the limit of zero volume fraction is certainly unattainable; instead there should be a fundamental limit that determines  $\phi_L$ , the lowest initial volume fraction of particles that will gel. The ultimate limitation is likely to be set by the mechanical strength of the fractal aggregates, which decreases as their size increases [4]. Ultimately, thermal fluctuations can deform and break the clusters, preventing gelation. Gravitational forces can also challenge their structural stability, since the body force due to gravity and the surface force due to hydrodynamic drag of sedimenting clusters result in a shear stress that can tear the aggregates apart. However, the elastic properties of large isolated aggregates are not well characterized experimentally, thus, the maximum stress that can be sustained by these aggregates has not been determined. As a result, the physical origin of the fundamental limitation to gelation and the value of  $\phi_L$  are not known.

In this Letter, we report results of experiments probing the limits to gelation. We use light scattering to measure dynamics of colloidal aggregates formed both in micro-

gravity and on Earth. We observe a crossover for fractal aggregates, from cluster diffusion at large length scales to internal elastic modes at short length scales. We show that gravitational stress limits the cluster growth on Earth, even under near buoyancy-matched conditions, whereas thermal fluctuations limit the growth of fractal structures in the absence of gravity. This allows us to determine the limits to colloid gelation.

We study the structure and dynamics of clusters using both static light scattering (SLS) and dynamic light scattering (DLS), exploring a wide range of length and time scales. For experiments in microgravity, we use the Physics of Colloids in Space (PCS) apparatus [5,6] on the International Space Station ISS. A narrow beam from a frequency-doubled Nd:YAG laser, with a wavelength  $\lambda = 532$  nm *in vacuo*, passes through the sample. Scattered light is collected from a volume of approximately  $10^{-5}$  cm<sup>3</sup> with a single-mode optical fiber, and detected with a solid state photon-counting detector; this fiber can be rotated to scattering angles ranging from  $11^\circ$  to  $169^\circ$ , probing scattering vectors  $3 \mu\text{m}^{-1} < q < 31 \mu\text{m}^{-1}$ . Additionally, a broad beam from a second Nd:YAG laser illuminates the sample in a direction perpendicular to the first beam. Scattered light from a larger volume of  $0.8$  cm<sup>3</sup> is imaged through a spherical lens onto a CCD camera to measure small-angle SLS or DLS at many wave vectors simultaneously,  $0.04 \mu\text{m} < q < 1.8 \mu\text{m}$ . We use polystyrene colloids with a particle size  $a = 10.5$  nm and  $\phi_0 = 8 \times 10^{-6}$ . The solvent is a nearly buoyancy-matching mixture of H<sub>2</sub>O and D<sub>2</sub>O which mitigates the effects of gravity, thereby allowing complementary studies of gelation on Earth, where we measure SLS and DLS over a comparable range of angles. Aggregation is initiated by mixing a MgCl<sub>2</sub> solution with the colloidal suspension to a final concentration of 42 mM. At this concentration, we expect aggregation to

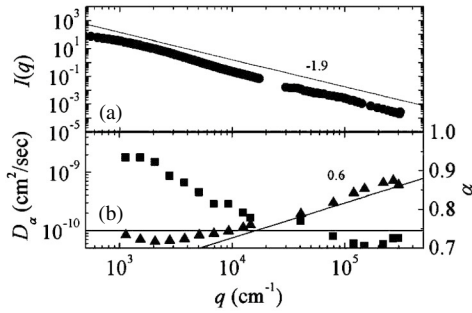


FIG. 1. (a) SLS; solid line is a guide to the eye showing that the fractal dimension is  $d_f = 1.9$ . (b) Effective diffusion coefficient  $D_\alpha$  ( $\blacktriangle$ ); solid lines are guides to the eye, with slopes 0 and 0.6; stretching exponent,  $\alpha$  ( $\blacksquare$ ), all 16 days after initialization.

be diffusion limited [7] and gelation to occur after  $\sim 90$  days [8].

Fractal clusters are formed, as evidenced by the power-law decay of the static scattering intensity,  $I(q)$ ; as a typical example, we show in Fig. 1(a) data obtained on the ISS, 16 days after aggregation was initiated. The fractal dimension is  $d_f = 1.9$ , in agreement with the value expected for DLCA [9–11]. The dynamic structure factor,  $f(q, \tau)$ , exhibits complete relaxation at all  $q$  and at all times, for both ground and space experiments. However, there is a qualitative change in the shape of the decay as  $q$  increases; the correlation functions deviate from exponential and become increasingly stretched exponential in form. To capture this behavior, we fit the data to a stretched exponential,  $f(q, \tau) \sim \exp(-[q^2 D_\alpha \tau]^\alpha)$ , where  $D_\alpha$  has the form of a diffusion coefficient, and  $\alpha$  is the stretching exponent. This form adequately captures the shape of the dynamic structure factor at all  $q$ , as shown by the solid curves in Fig. 2, where we plot  $f(q, \tau)$  for the same sample shown in Fig. 1(a).

There is a distinct crossover between the high- and low- $q$  regimes, which is most clearly seen in the  $q$  dependence of the fitting parameters  $D_\alpha$  and  $\alpha$ , shown in Fig. 1(b). At low  $q$ ,  $D_\alpha$  is essentially  $q$  independent, whereas, at high  $q$ , it increases, asymptotically scaling as  $D_\alpha \sim q^{0.6}$ . Concurrently, there is a change in the degree of stretching of  $f(q, \tau)$ , characterized by  $\alpha$  decreasing from nearly 1 at low  $q$  to about 0.7 at high  $q$ . The deviation from low- $q$  behavior takes place at wave vectors near the limit of the fractal scaling range of the SLS data shown in Fig. 1(a). We can observe this crossover because we access a large range of scattering vectors, corresponding to length scales on the order of and smaller than the cluster size.

For all aggregation times,  $D_\alpha$  is nearly  $q$  independent and  $\alpha \sim 1$  at low  $q$ , reflecting diffusive motion of clusters; moreover, the complete decay of  $f(q, \tau)$  indicates that the sample remains ergodic. Thus, within our experimentally

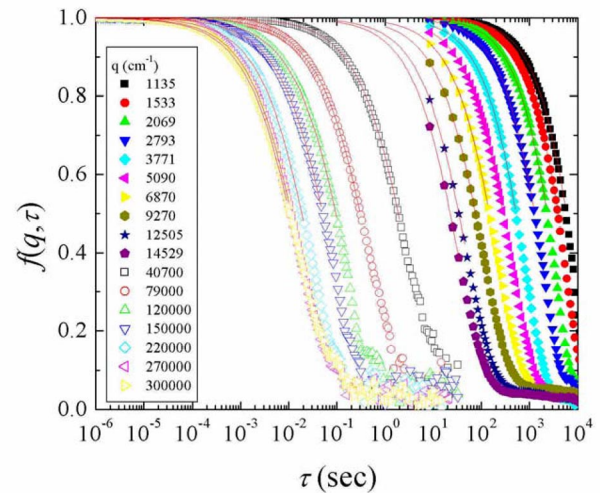


FIG. 2 (color online). Correlation functions from DLS measurements taken 16 days after initialization over a range of scattering vectors  $1.1 \times 10^3 < q < 3 \times 10^5 \text{ cm}^{-1}$ . Solid curves are stretched exponential fits to the data.

accessible time, the sample does not gel, but instead remains a suspension of freely diffusing fractal aggregates. To estimate the cluster size, we determine the first cumulant of  $f(q, \tau)$ ,  $\Gamma_1$ , for the small-angle scattering data and calculate the effective diffusion coefficient,  $D_{\text{eff}} = \Gamma_1/q^2$  [12]. As shown in Fig. 3(a),  $D_{\text{eff}}$  exhibits pronounced  $q$  dependence. This reflects the effect of rotational motion, which makes a significant contribution to the dynamics for  $q > q_c$ , where  $q_c = 2\pi/R_c$ ; because of the heterogeneous structure of the fractal clusters, the scattered intensity of a single cluster varies upon rotation, leading to a faster decay of  $f(q, \tau)$  [13]. However, because

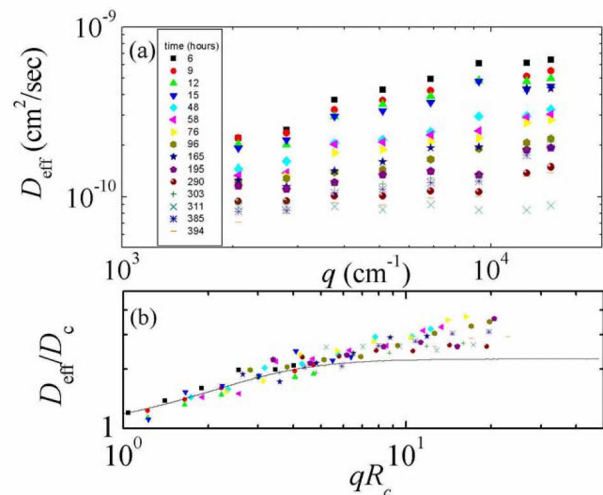


FIG. 3 (color online). (a)  $D_{\text{eff}}$  from cumulant fits at different aggregation times and (b) scaling of  $D_{\text{eff}}$  along diagonal onto a single master curve for microgravity data (symbols). Solid line shows theoretical curve from 15.

of the scale invariance of the fractal structure, the data can be scaled onto a single master curve; this is accomplished by normalizing  $D_{\text{eff}}$  by  $D_c$ , the translational diffusion coefficient of clusters with average size,  $R_c$ , and plotting them as a function of  $qR_c$ . The data scale onto a master curve remarkably well and are in agreement with the theoretical prediction at low  $q$ , as shown in Fig. 3(b), allowing an accurate measure of the average cluster size and its time evolution from the low- $q$  dynamics.

For contributions of rotational and translational diffusion alone, we expect  $D_{\text{eff}}$  to plateau at very large  $q$ ; this, however, is not observed experimentally. The deviation between the scaled experimental data and the theoretical prediction for  $qR_c > 10$  must reflect the contribution of internal fluctuations within the cluster [13]. Such internal dynamics has been observed in colloidal gels [14], where the fractal clusters are constrained by the network and thus can neither translate nor rotate. In this case,  $f(q, \tau)$  is well described by a stretched exponential form with an exponent  $\alpha \sim 0.7$ , which results in a  $q$  dependence for the apparent diffusion coefficient,  $D_\alpha \sim q^{2-2\alpha} = q^{0.6}$ . This is in striking agreement with the measured values of  $\alpha \sim 0.7-0.8$  and  $D_\alpha \sim q^{0.6}$ , and confirms that the high- $q$  dynamics probe internal fluctuations of the clusters. It also accounts for the crossover behavior observed in Fig. 1(b). Thus, although our sample is not a gel, the incredibly slow diffusion of the clusters allows us to measure their internal dynamics.

The internal dynamics probed at high  $q$  provide previously inaccessible information about the elasticity of individual clusters. As a cluster grows larger, it also becomes floppier, resulting in internal fluctuations with larger amplitudes and slower relaxations. The motion of a segment of the cluster of size  $q^{-1}$  is determined by integrating over thermal fluctuations of all length scales greater than  $q^{-1}$  up to the cluster size. The dominant contribution to this motion stems from the elastic mode with the largest wavelength, whose length is the size of the cluster itself. In the case of fractal gels, the resultant dynamic structure factor is well approximated at short times by  $f(q, t) = \exp(-q^2 D_p t^p)$ , where  $p$  is the stretching exponent, and  $D_p = F(R_c) \kappa_0^{-(1-p)}$ , with  $F(R_c)$  a function of the average cluster size [14]. Thus,  $D_p$  reflects the motion due to the internal modes and depends weakly on the particle-particle spring constant,  $\kappa_0$ . However, to correctly describe the dynamics of large isolated clusters at high  $q$ , we must also include the contributions of both translational and rotational diffusion, which are small but nonnegligible. We therefore refine the fitting function by adding a diffusive term,  $f(q, t) = \exp[-q^2(D_p t^p + D_{\text{eff}} t)]$ , where  $D_{\text{eff}}$  includes contributions from both rotational and translational diffusion of the clusters. We use the value for DLCA clusters in the high- $q$  limit,  $D_{\text{eff}} = 2.2D_c$  [15], and allow  $D_p$  and  $p$  to vary. From the fit, we

find that each parameter is independent of both  $q$  and  $R_c$ ; moreover, their values are quantitatively consistent with those found for gelled samples of the same particles, prepared at high  $\phi_0$ . We estimate  $\kappa_0 = 5 \times 10^3$  dyn/cm, a value in reasonable agreement with  $\kappa_0 = 1.5 \times 10^4$  dyn/cm measured by rheology and light scattering on gelled samples [14,16]. These results demonstrate that the internal fluctuations of isolated clusters can be described using the same models developed for colloidal gels.

We compare the aggregation kinetics measured in space with those measured on Earth in Fig. 4. In microgravity the clusters grow at a rate in excellent qualitative agreement with that expected for DLCA,  $R_c \sim t^{1/d_f}$ . This cluster growth persists for the full duration of the space experiment; gelation is not observed because the duration is less than the gelation time,  $t_{\text{gel}} \sim 90$  days, estimated by extrapolating the observed growth to the cluster size expected at the gel point,  $R_c = 450 \mu\text{m}$ . By contrast, the time evolution of  $R_c$  on Earth shows significant deviation from the behavior anticipated for DLCA. The initial growth of the clusters is identical to that in space, following a power-law time evolution consistent with DLCA; however, after  $\sim 10$  h, the growth deviates from the expected behavior and reaches a plateau, with no further growth observed. Thus, this system will not gel as the maximum cluster size  $R_c \sim 20 \mu\text{m}$  is more than 1 order of magnitude lower than that needed to form a gel.

This arrested cluster growth observed on Earth suggests that gravity can ultimately limit gelation. As an aggregate sediment, its buoyant weight is balanced by hydrodynamic drag from the fluid [4]. Hydrodynamic resistance acts primarily at the surface of the cluster, but is screened in the interior, whereas gravity is a body force distributed throughout the cluster. This results in an internal shear stress across the cluster. The response of the cluster is equivalent to that of a spring, resulting in a strain of order  $\gamma_g = Mg/\kappa_c R_c$  [4], where the gravitational acceleration is  $g$ , and the buoyant mass of the cluster is  $M = M_0(R_c/a)^{d_f}$ , with  $M_0 = 4\pi a^3 \Delta\rho/3$  the buoyant mass of a single colloidal particle with a density

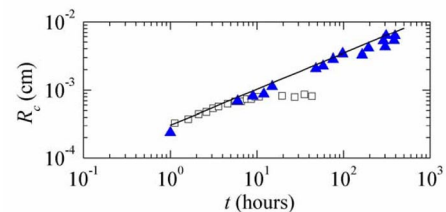


FIG. 4 (color online). Cluster size as a function of aggregation time; data at early times corrected for estimated rotational contributions for  $10^{-2}g$  ( $\square$ ) and at late times from scaling of  $D_{\text{eff}}$  for  $10^{-6}g$  ( $\blacktriangle$ ). Solid line shows expected growth from DLCA.

mismatch of  $\Delta\rho$ . The cluster spring constant is given by  $\kappa_c = \kappa_0(a/R_c)^\beta$ , where  $\beta = 2 + d_B$  is the elasticity exponent, and  $d_B$  is the bond dimension, whose value is  $d_B = 1.1$  for DLCA clusters [17]. Thus, the strain on the cluster is given by  $\gamma_g = M_0g(R_c/a)^{\beta+d_f}/(R_c\kappa_0)$ . There are inevitably inherent uncertainties in matching the density of the colloidal particles to that of the fluid; in our experiment, uncertainties in the relative volumes of H<sub>2</sub>O and D<sub>2</sub>O, as well as ambient temperature fluctuations, lead to a buoyancy mismatch, which we estimate to be  $\Delta\rho \sim 10^{-3}$  g/cm<sup>3</sup>. Colloidal aggregate gels are found to irreversibly and catastrophically break under external strains of  $\gamma > 0.45$ , independent of  $\phi_0$  [16]. Thus, the critical strain is reached for a cluster size of  $R_c \sim 35$   $\mu\text{m}$ , which is in excellent agreement with the observed arrest in growth on Earth,  $R_c \sim 20$   $\mu\text{m}$ . Thus, gravity ultimately limits cluster growth on Earth.

In microgravity, the gravitationally induced strains are 6 orders of magnitude smaller; consequently, the clusters can grow to be much larger. Instead, strain induced by thermal fluctuations will eventually limit growth of fractal clusters, and thus will ultimately limit gelation [4]. The elastic energy of a fractal is  $E_e = \kappa_c u^2/2$  for a linear displacement  $u$ ; therefore, thermal fluctuations produce a strain of  $\gamma_T = (k_B T(R_c/a)^{d_B}/(a^2\kappa_0))^{1/2}$ . Thermal fluctuations set the maximum cluster size to  $R_T \sim 1.2 \times 10^2$   $\mu\text{m}$ . This is close to the maximum cluster sizes observed in the microgravity experiment; indeed, we observe signs of a plateau in  $R_c$  near the end of the experiment.

The fractal nature of the aggregates is essential to enable a small volume fraction of colloids to form a connected solid, thus any deviation from fractal growth severely compromises gelation. On Earth, gravity limits the maximum cluster size, thereby determining the minimum volume fraction which will gel. Since the cluster size at gelation is  $R_c = a\phi_0^{1/(d_f-3)}$ ,  $\phi_L = (\gamma_m a \kappa_0 / M_0 g)^{(\beta+d_f-1)/(d_f-3)}$ ; for our samples on Earth,  $\phi_L = 9 \times 10^{-5}$ . Consistent with this, visual observations of samples over a range of volume fractions,  $4 \times 10^{-4} < \phi_0 < 8 \times 10^{-6}$ , show that for  $\phi_0 < 10^{-4}$  samples appear heterogeneous, suggesting that gelation is compromised. By contrast, in microgravity, thermally induced strains limit the cluster size, setting  $\phi_L =$

$(\gamma_m^2 a^2 \kappa_0 / k_B T)^{(d_f-3)/d_B}$ . For our microgravity experiments, this leads to  $\phi_L \approx 3 \times 10^{-5}$ . Similar limitations pertain for all materials, even if the individual chains are stronger. Thus, the fundamental limitation to gelation is determined by thermal fluctuations; their magnitude ultimately becomes so large that they inhibit further fractal growth of the clusters, thereby preventing gelation.

This work was supported by NASA (NAG3-2284).

\*Current Address: GPC cc 26, Universite Montpellier II, P. E. Bataillon, Montpellier 34000, France.

†Current Address: Scitech Instruments, Inc., North Vancouver, BC V7J 2S5, Canada.

‡Current Address: Department of Physics, University of Konstanz, Konstanz, Germany.

§Current Address: Department of Chemical Engineering, UCSB, Santa Barbara, CA, USA.

||Current Address: NASA Marshall Space Flight Center, Huntsville, AL 35812, USA.

- [1] D. A. Weitz *et al.*, Phys. Rev. Lett. **53**, 1657 (1984).
- [2] M. Carpineti and M. Giglio, Phys. Rev. Lett. **68**, 3327 (1992).
- [3] J. Bibette *et al.*, Phys. Rev. Lett. **69**, 981 (1992).
- [4] Y. Kantor and T. A. Witten, J. Phys. (Paris) Lett. **45**, L675 (1984).
- [5] C. T. Lant *et al.*, Appl. Opt. **36**, 7501 (1997).
- [6] M. P. Doherty *et al.*, NASA Technical Report No. NASA/TM-2002-211371, 2002.
- [7] M. Carpineti *et al.*, Phys. Rev. Lett. **42**, 7347 (1990).
- [8] Collection of data at longer times was precluded due to limitations of the ISS experiment.
- [9] D. A. Weitz *et al.*, Phys. Rev. Lett. **54**, 1416 (1985).
- [10] M. Carpineti and M. Giglio, Phys. Rev. Lett. **70**, 3828 (1993).
- [11] D. Asnaghi *et al.*, Phys. Rev. A **45**, 1018 (1992).
- [12] B. J. Berne and R. Pecora, *Dynamic Light Scattering* (Wiley, New York, 1976).
- [13] H. M. Lindsay *et al.*, Phys. Rev. A **39**, 3112 (1989).
- [14] A. H. Krall and D. A. Weitz, Phys. Rev. Lett. **82**, 1064 (1998).
- [15] M. Y. Lin *et al.*, J. Phys. Condens. Matter **2**, 3093 (1990).
- [16] T. Gisler, R. C. Ball, and D. A. Weitz, Phys. Rev. Lett. **82**, 1064 (1999).
- [17] P. Meakin, J. Phys. A **17**, L975 (1984).

## Time-Dependent Strength of Colloidal Gels

S. Manley,<sup>1</sup> Benny Davidovitch,<sup>2</sup> Neil R. Davies,<sup>1</sup> L. Cipelletti,<sup>1,\*</sup> A. E. Bailey,<sup>1,†</sup> R. J. Christianson,<sup>1</sup> U. Gasser,<sup>1,‡</sup> V. Prasad,<sup>1,§</sup> P. N. Segre,<sup>1,||</sup> M. P. Doherty,<sup>3</sup> S. Sankaran,<sup>3</sup> A. L. Jankovsky,<sup>3</sup> B. Shiley,<sup>4</sup> J. Bowen,<sup>4</sup> J. Eggers,<sup>4</sup> C. Kurta,<sup>4</sup> T. Lorik,<sup>4</sup> and D. A. Weitz<sup>1</sup>

<sup>1</sup>*Department of Physics & DEAS, Harvard University, Cambridge, Massachusetts 02138, USA*

<sup>2</sup>*DEAS, Harvard University, Cambridge, Massachusetts 022138, USA*

<sup>3</sup>*NASA Glenn Research Center, Brook Park, Ohio 44135, USA*

<sup>4</sup>*Zin Technologies, Inc., Brook Park, Ohio 44142, USA*

(Received 27 July 2004; published 22 July 2005)

Colloidal silica gels are shown to stiffen with time, as demonstrated by both dynamic light scattering and bulk rheological measurements. Their elastic moduli increase as a power law with time, independent of particle volume fraction; however, static light scattering indicates that there are no large-scale structural changes. We propose that increases in local elasticity arising from bonding between neighboring colloidal particles can account for the strengthening of the network, while preserving network structure.

DOI: [10.1103/PhysRevLett.95.048302](https://doi.org/10.1103/PhysRevLett.95.048302)

PACS numbers: 82.70.Gg, 61.43.Hv, 62.20.Dc, 82.70.Dd

Gels are dilute connected networks which are capable of supporting applied stresses; they are commonly used to control the rheological properties of complex materials. Such networks can be formed by the aggregation of colloidal particles, which occurs when an attractive interaction is induced between them. Network elasticity is highly sensitive to the connectivity and arrangement of particles in the constituent aggregates. Colloidal gels are out-of-equilibrium systems; as a result, these networks frequently display time-dependent properties, due to network restructuring. This kind of aging is modeled for generic nonequilibrium systems as an evolution toward lower energy states, as the system explores a complex energy landscape [1,2]. However, network elasticity is also dependent on the interactions between particles; therefore, time-dependent interactions may also lead to changes in network properties. For colloidal gels, it is generally assumed that interparticle attractions, such as those described by Derujaguin-Landau-Verwey-Overbeek [3,4] or Asakura-Oosawa potentials [5], determine local bond elasticity, thus, in principle, limiting their strength [6,7]. In the absence of a steric stabilization layer, particle interactions can also arise from physical bonds, as a result of covalent bonding or polymer entanglements. Within this framework, time evolution of network properties can be linked to the interparticle potential, for example, through the transport of particles from secondary to primary minima [8]. Aging can also be a consequence of time-dependent physical bonding; for example, the sintering of aggregated polystyrene particles is thought to drive local shrinkage that deforms the network [9]. The strength of the local interparticle bonds will have a direct impact on the network elasticity; however, these critical effects have never been explored.

In this Letter, we present measurements of the elasticity of colloidal silica gels. Surprisingly, we find that, upon gelation, their storage moduli  $G'$  increase as a power law in

time,  $G' \sim t^{0.4}$ , independent of initial volume fraction  $\phi$ . Moreover, the time evolution of the network persists long after gelation occurs, for the duration of the measurement. As a consequence, their elasticity maintains the same volume fraction dependence,  $G' \sim \phi^{3.6}$ , independent of time. We postulate that the stiffening of the network is a result of chemical reactions at the junctions between neighboring particles, which increase local bond strength. We introduce a simple model based on increasing local bond area to account for the observed data.

We use charge-stabilized silica colloids with a radius  $a = 10$  nm in water at 25 °C; we initiate aggregation by adding  $\text{MgCl}_2$  to a concentration of 40 mM. Gravitational loading may induce network restructuring since  $\Delta\rho = 1.27$  g/cm<sup>3</sup>. To circumvent this, we perform experiments in microgravity. We study a gel at  $\phi = 2 \times 10^{-4}$ ; this is in the range of concentration where aging is observed in polystyrene gels [9]. For experiments in microgravity, we use the Physics of Colloids in Space apparatus on the International Space Station (ISS) [10,11]. To form the sample in space, the salt and colloid solutions are stored in separate chambers, sealed with a pinch valve. When the valve is released, two metal rods push in an alternating fashion on the rubber fluid bladders backing the chambers to mix the solutions.

To obtain information about the structure and elasticity of colloidal gels at low  $\phi$ , we perform both static light scattering (SLS) and dynamic light scattering (DLS) over a wide range of angles [12]. The aggregation process results in a relatively monodisperse size distribution of clusters, which is reflected by a peak in the static scattering intensity  $I(q)$ ; this peak shifts to a lower wave vector  $q$  and increases in intensity as clusters grow [13]. Fractal clusters are formed, as evidenced by the power law decay of  $I(q)$ ; we show in Fig. 1 (inset) data obtained on the ISS, for different times after aggregation was initiated. The fractal dimen-

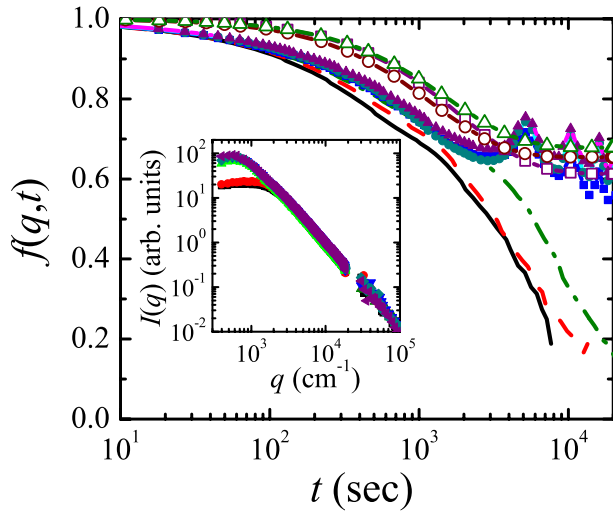


FIG. 1 (color online). Dynamic structure factors at  $q = 3771 \text{ cm}^{-1}$ ; raw data at 12 (solid line), 18 (dashed line), 40 (dash-dotted line), 55 (■), 69 (●), and 93 h (▲) since initialization and corrected for external temperature fluctuations at 55 (□), 69 (○), and 93 h (△). Inset: Static light scattering between 1 and 65 h after initialization. No changes are observed after  $\sim 15$  h.

sion is  $d_f = 1.9$ , consistent with aggregation that may begin slightly in the reaction-limited regime, but crosses rapidly into diffusion-limited cluster aggregation (DLCA) [14,15]. Roughly 12 h after initialization, the SLS stops evolving in time. This is consistent with the onset of gelation, which occurs when the colloidal aggregates grow large enough to form a space-filling network. For DLCA gels, the average cluster size at gelation is  $R_c = a\phi_0^{1/(d_f-3)}$  [16]. We calculate  $R_c = 2.3 \times 10^{-3} \text{ cm}$  for our sample; this corresponds to a wave vector  $q = 1360 \text{ cm}^{-1}$ , and is in good agreement with the final position of the peak of  $I(q)$ .

Gels at such low  $\phi$  are extremely weak, and cannot support the stresses necessary for typical bulk rheological measurements. Instead, we measure the dynamic structure factor,  $f(q, \tau)$ , which provides information about their structural relaxation, and hence their elasticity. Even after SLS suggests that the sample is a gel,  $f(q, \tau)$  still shows a complete relaxation at  $q = 3771 \text{ cm}^{-1}$ , as shown by the data plotted as lines in Fig. 1. As the sample ages, its relaxation time increases, as seen for  $t = 40$  h after initialization. At even longer times, the decay becomes arrested. The resultant dynamic structure factor is approximated by  $f_g(q, \tau) = \exp(-q^2 \langle \Delta r^2 \rangle / 6)$ , where the mean squared displacement of a segment of the gel,  $\langle \Delta r^2 \rangle = \delta^2 (1 - \exp[-(\tau/\tau_0)^\mu])$ , results from its overdamped modes, with  $\tau_0$  the viscous damping time, and  $\delta^2$  the maximum deviation [17]. At long delay times, particle motions are constrained by the network; thus, the dynamics saturate to a plateau when the maximum mean

squared displacement is less than  $1/q$ . In these experiments performed on the ISS, an unusual oscillation is seen on top of the developing plateau. Its period is independent of  $q$ , and corresponds to the 83 min orbital period of the ISS; temperature sensors located near the apparatus record an oscillation of the same period. We therefore correct the correlation functions by fitting to a convolution of  $f_g(q, \tau)$  with an oscillatory function with a period of 83 min. The fit parameters allow us to determine the unperturbed  $f_g(q, \tau)$ , shown in Fig. 1 as open symbols. The plateau height  $f_g(q, \tau = \infty)$  increases with sample age; thus, the particle displacements become increasingly constrained over time, consistent with an increase in gel elasticity. By contrast, SLS shows that no significant changes in the structure of the gel occur over the same time period.

To determine the generality of this aging behavior, we investigate the evolution of the network at higher  $\phi$ ; this has the advantage that the elastic moduli are large enough to be measured directly with a rheometer. We perform measurements on Earth for  $0.01 < \phi < 0.05$ ; at these volume fractions, gels maintain their structural integrity under gravity over months. The DLCA gel time is relatively short, of the order of a few seconds; and in order to avoid heterogeneity in the networks, we reduce the salt concentration to 15 mM. We measure both storage and loss moduli,  $G'$  and  $G''$ , with a strain-controlled rheometer in an oscillatory-shear experiment using a double-walled Couette geometry. Measurements at fixed frequency under increasing strain amplitude show a linear elastic response at low strains, with a yield strain of 0.3. We measure the frequency-dependent  $G'$  and  $G''$  for different  $\phi$  using a fixed strain amplitude of  $\gamma = 5 \times 10^{-3}$ , well within the linear regime. The measured values of  $G'$  are about an

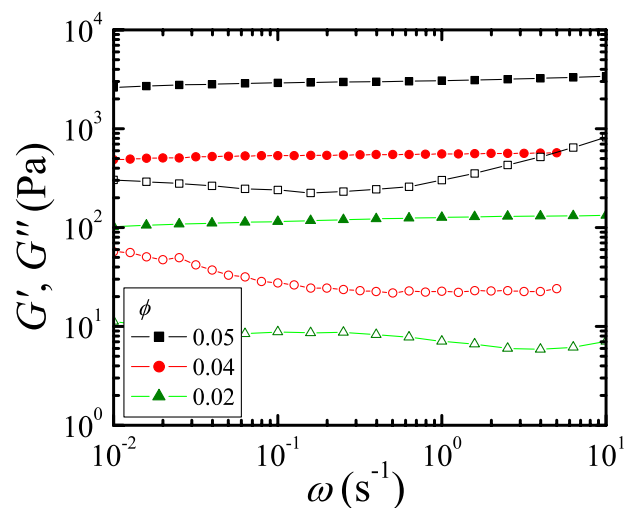


FIG. 2 (color online). Linear storage (filled symbols) and loss (open symbols) moduli for different volume fractions at strain amplitude  $\gamma = 5 \times 10^{-3}$ .

order of magnitude larger than  $G''$  for all  $\phi$  as shown in Fig. 2, demonstrating that these gels are indeed solid networks.

To determine the time evolution of the gels, we measure  $G'$  and  $G''$  at fixed strain amplitude  $\gamma = 5 \times 10^{-3}$  and frequency  $\omega = 1$  rad/s over a period of 12 h, beginning upon gelation, as determined by the dominance of  $G'$  over  $G''$ . The samples all become stiffer with time, consistent with the development of a plateau in the DLS in the ISS experiment. At these higher  $\phi$ , the time evolution can be more precisely determined; for each of the samples, we find a power-law growth,  $G' \sim t^{0.4}$ , over the entire measurement time, as shown in Fig. 3. To ascertain that the oscillatory strain does not influence the aging, we measure the modulus of the sample with  $\phi = 0.02$  only once every 30 min, allowing the sample to remain quiescent between measurements. The time dependence is unchanged, confirming that the strains applied do not affect  $G'$ .

The elasticity of fractal colloidal gels is strongly  $\phi$  dependent. However, the time dependence of  $G'$  is independent of  $\phi$ , and the data can all be scaled together; thus, the  $\phi$  dependence of  $G'$  is directly reflected by the scale factor  $\beta$ . The dependence  $\beta^{-1} \sim \phi^{3.6}$ , shown in Fig. 3 (inset) is remarkably similar to that expected for fractal gels, where the macroscopic modulus is governed by the stiffness of the aggregate network. The elasticity of a fractal aggregate of size  $R_c$  is determined by the spring constant  $\kappa(R_c) = \kappa_0 a^2 / N R_c^2$  of its backbone, where  $\kappa_0$  is the interparticle spring constant and  $N$  is the number of particles in the chain [15,18]. This expression can be understood in an intuitive way, if one assumes that the primary contributions to elasticity are from bond bending. For a bent chain, a change in the length of the chain  $\Delta l$  is translated into a change in the average local bending angle  $\langle \Delta \theta \rangle$ , resulting in an elastic energy of  $U = \frac{1}{2} \kappa_0 (a \langle \Delta \theta \rangle)^2 N$ .

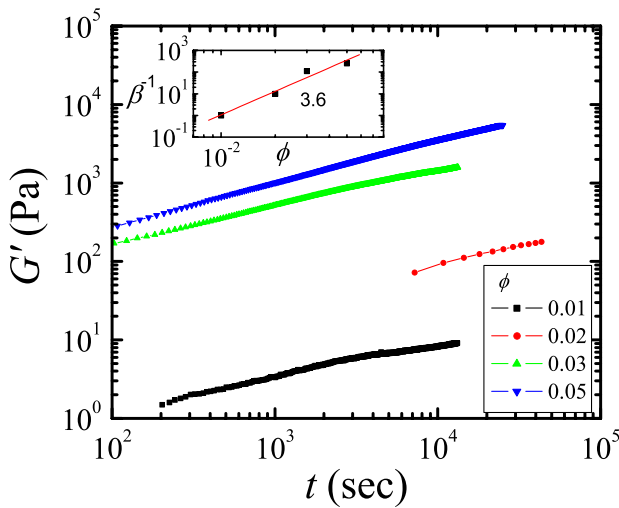


FIG. 3 (color online). Growth of the linear storage modulus  $G'$  with time for different volume fractions. Scale factors  $\beta$  used to shift  $G'$  onto a single master curve (inset).

The total change in angles is  $N \Delta \theta = \frac{\Delta l}{R_c}$ , which is shared among all of the  $N = R^{d_b}$  particles in the chain, where  $d_b$  is the bond dimension. The spring constant therefore depends inversely on  $R_c^2$ , and inversely on  $N$ . The elastic modulus of the gel is then  $G' = \frac{\kappa(R_c)}{R_c} = \frac{\kappa_0}{a} \phi^{(3+d_b)/(3-d_f)}$ ; using  $d_b = 1.1$  as found in simulations [19], and  $d_f = 1.9$ , we obtain an exponent of 3.7, in excellent agreement with our data.

The weakest link determines  $\kappa_0$ ; we assume that this is the contact region between particles, which is a neck of size  $r_0$ , whose elastic properties are the same as that of the particles, as shown schematically in Fig. 4. The strain,  $\gamma$ , imposed by the bending of the necks, will be concentrated in a region of size  $r_0^3$ , resulting in a strain energy of  $E \gamma^2 r_0^3$ , where  $E$  is the Young's modulus of silica. A change in bond angle of  $\Delta \theta$  will result in a change in elastic energy of  $\kappa_0 (a \Delta \theta)^2$ ; thus, the local spring constant is  $\kappa_0 = E r_0$ . This allows us to relate the properties of the local bonds to the macroscopic modulus, and to deduce how changes in local bonding result in changes in network elasticity. At the microscopic level, either an increase in contact radius, or an increase in elasticity of the material in the contact region will lead to an increase in  $\kappa_0$ .

We assume that upon gelation particles form contacts at the molecular level. Particles in contact gain surface energy by deforming elastically, thereby increasing their contact area as described by the Johnson-Kendall-Roberts (JKR) theory [20]. The radius of the contact area reaches a maximum value,  $r_m$ , determined by a balance between elastic deformation and surface energies:  $r_m \approx (9 \sigma a^2 / 4 E)^{1/3}$ , where  $\sigma$  is the surface tension. Substituting typical values for silica of  $\sigma \approx 100$  mJ/m<sup>2</sup> and  $E \approx 10^{10}$  Pa, we obtain  $r_m \approx 1.3$  nm. Using the expression for the modulus, we calculate  $G' \approx 2 \times 10^4$  Pa, for a gel at  $\phi = 0.05$ . This is approximately twice the measured  $G'$  after 24 h, indicating that the JKR contact may be still developing, consistent with the observation that  $G'$  continues to increase during the entire measurement time.

The time dependence of  $G'$  is  $\phi$  independent, and SLS indicates that there is no change in the gel structure. This

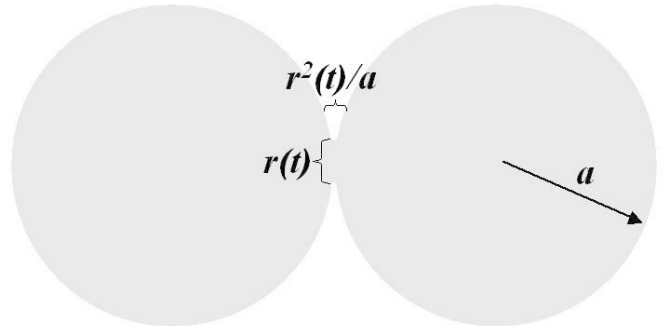


FIG. 4. Schematic of two sintering spheres.

suggests that it is a time-dependent interparticle spring constant  $\kappa_0(t)$  and not structural changes, that is responsible for increases in  $G'$ . We assume that this time dependence arises from an increase in the size of the neck. One possibility is that this growth occurs by mass transfer; however, this is too slow to explain the observed growth in  $G'$ . Instead, we hypothesize that the kinetics of bond formation is reaction limited, as formation of Si-O-Si bonds requires hydration of cations at the surface of the particles. Support for this comes from atomic force microscopy studies [21], which attribute a short-ranged repulsion to the presence of a counterion layer. We can use the measurements of  $G'(t)$  to estimate the bond activation energy, and the evolution of the contact area. The number of bonds required to make a JKR contact is  $N_m \sim r_m^2$ , and we estimate that the time scale for a bond to form is  $\tau \approx A_f^{-1} e^{-\Delta U/k_B T}$ , where  $A_f \approx 10^{-13} \text{ sec}^{-1}$  is a molecular attempt frequency. The rate of formation of new bonds is  $\frac{dN}{dt} \approx (N_m - N)/\tau \approx N_m/\tau$  for  $N \ll N_m$ . Since  $r \sim \sqrt{N}$ , its time evolution is  $r \approx r_0 \sqrt{t/\tau}$ , where  $r_0$  is the contact radius upon gelation. Substituting  $r$  into our expressions for  $\kappa_0$  and  $G'$ , we obtain  $G' \sim t^{0.5}$ , in reasonable agreement with our measurement,  $G' \sim t^{0.4}$ . The time dependence requires  $\Delta U \approx 33k_B T$ ; this is comparable to known hydration enthalpies [21], supporting our hypothesis.

An alternative microscopic picture for the strengthening of the gel network is an increase in the elasticity of the bonded region. Hydrated silica surfaces are swollen relative to dry ones [22]; this could be due to a gel-like surface layer, composed of “polymeric” chains of  $-\text{Si}(\text{OH})_2\text{-O-Si}(\text{OH})_2\text{-OH}$  groups. Measurements made in humid air indicate that bond strength also increases with contact time [22], purportedly as a result of consolidation of the gel layer. It is conceivable that, in water, this would lead to an increase in  $E$ , and therefore  $\kappa_0(t)$ ; however, the nature of these effects is unclear, and difficult to quantify.

Our measurements show that changes in bonding at the particle level can significantly affect the macroscopic elasticity of colloidal gels. While the focus here is on silica gels, we expect similar behavior for gels of different materials. This is in sharp contrast with the more usual time evolution of elasticity due to changes in the network structure; this provides an alternate potential means for changing the time-dependent materials properties of colloidal gels.

This work was supported by NASA (NAG3-2284).

- 
- \*Present address: GDPC cc 26, Universite Montpellier II, P. E. Bataillon, Montpellier 34000, France.  
 †Present address: Scitech Instruments, Inc., North Vancouver, BC, Canada V7J 2S5.  
 ‡Present address: Dept. of Physics, University of Konstanz, Konstanz, Germany.  
 §Present address: Dept. of Chemical Engineering, UCSB, Santa Barbara, CA 93106, USA.  
 ||Present address: NASA Marshall SpaceFlight Center, Huntsville, AL 35812, USA.
- [1] B. Rinn, P. Maass, and J.-P. Bouchaud, *Phys. Rev. B* **64**, 104417 (2001).
  - [2] P. G. Debenedetti and F. H. Stillinger, *Nature (London)* **410**, 259 (2001).
  - [3] B. V. Derjaguin and L. Landau, *Acta Physicochim URSS* **14**, 633 (1941).
  - [4] E. J. W. Verwey and J. T. G. Overbeek, *Theory of Stability of Lyophilic Colloids* (Elsevier, Amsterdam, 1948).
  - [5] S. Asakura and F. Oosawa, *J. Chem. Phys.* **22**, 1255 (1954).
  - [6] W. Y. Shih, W.-H. Shih, and I. A. Aksay, *J. Am. Ceram. Soc.* **82**, 616 (1999).
  - [7] V. Prasad *et al.*, *Faraday Discuss.* **123**, 1 (2003).
  - [8] H. M. Wyss *et al.*, *J. Colloid Interface Sci.* **241**, 89 (2001).
  - [9] L. Cipelletti *et al.*, *Phys. Rev. Lett.* **84**, 2275 (2000).
  - [10] C. T. Lant *et al.*, *Appl. Opt.* **36**, 7501 (1997).
  - [11] M. P. Doherty *et al.*, NASA Technical Report No. NASA/TM-2002-211371 (2002).
  - [12] S. Manley *et al.*, *Phys. Rev. Lett.* **93**, 108302 (2004).
  - [13] M. Carpineti *et al.*, *Phys. Rev. A* **42**, 7347 (1990).
  - [14] M. Carpineti and M. Giglio, *Phys. Rev. Lett.* **68**, 3327 (1992).
  - [15] T. Gisler, R. C. Ball, and D. A. Weitz, *Phys. Rev. Lett.* **82**, 1064 (1999).
  - [16] M. Carpineti and M. Giglio, *Phys. Rev. Lett.* **70**, 3828 (1993).
  - [17] A. H. Krall and D. A. Weitz, *Phys. Rev. Lett.* **80**, 778 (1998).
  - [18] Y. Kantor and I. Webman, *Phys. Rev. Lett.* **52**, 1891 (1984).
  - [19] P. Meakin *et al.*, *J. Phys. A* **17**, L975 (1984).
  - [20] K. Johnson, K. Kendall, and A. Roberts, *Proc. R. Soc. A* **324**, 301 (1971).
  - [21] I. U. Vakarelski, K. Ishimura, and K. Higashitani, *J. Colloid Interface Sci.* **227**, 111 (2000).
  - [22] G. Vigil *et al.*, *J. Colloid Interface Sci.* **165**, 367 (1994).

# Crystallization Kinetics of Binary Colloidal Alloys

R.J. Christianson, U. Gasser, A. E. Bailey, V. Prasad, S. Manley, P.N. Segre, L. Cipelletti, and D.A. Weitz  
*Department of Physics and Division of Engineering and Applied Sciences, Harvard University, Cambridge, MA*

A.B. Schofield and P.N. Pusey  
*School of Physics, The University of Edinburgh, Edinburgh, UK*

M.P. Doherty, S. Sankaran, A.L. Jankovsky, B. Shiley, J. Bowen, K. Dendorfer, J. Eggers, C. Kurta, and T. Lorik  
*NASA Glenn Research Center, Brookpark, OH*

(Dated: November 5, 2004)

Binary alloy colloidal crystals have significantly different crystallization kinetics than do those comprised of a single species. However, differential sedimentation has precluded accurate study of this behavior. We present the first results on undisturbed crystallization kinetics of hard-sphere binary mixtures, obtained on the International Space Station, where the deleterious effects of gravity are eliminated. We study samples which crystallize in the  $AB_{13}$  structure, and other samples which form  $AB_6$  BCC, a heretofore unreported colloidal crystal structure. Both structures exhibit induction times longer than those typically seen in one-component systems, followed by anomalous slow ripening behavior. This suggests competition between kinetics of demixing and formation of ordered binary crystalline structures.

The free energy of hard-spheres is exclusively entropic; thus, one might expect these systems to remain in a disordered state. Countering this naive intuition, suspensions of monodisperse hard-sphere colloidal particles crystallize at volume fractions above 0.494 [1, 2]. Crystallization occurs because the ordered packing of the spheres increases the total free volume of the system, thereby increasing the total entropy, even though the configurational entropy associated with the average particle positions is decreased. Crystallization of monodisperse hard spheres provides a convenient and easily studied model of crystallization of atomic systems; it is also of fundamental interest for the study of the packing of spheres, and as a phase transition with coupled conserved and non-conserved order parameters [3–8]. There is also great practical potential of ordered colloidal structures for photonic devices [9].

This potential is even greater for the use of crystals comprised of two different sizes of particles; such binary alloy crystals greatly increase the diversity of available structures for photonic applications. In addition, study of their crystallization provides heretofore unattainable insight into the behavior of two-component atomic crystals such as binary metallic alloys. However, very little is understood about the nature of the crystallization of binary mixtures of hard spheres. The maximization of the total entropy of the system becomes much more complex when two different sizes of particle are present, and the nature of the packing of binary mixtures remains poorly understood. Below a size ratio of 0.2, phase separation of the two components is always predicted [10]. However, at higher size ratios, the configurational entropy gained from keeping the two components intermingled becomes more important. This leads to a diverse array of phase behaviors as the size and number

ratios of the two components are varied [11–15]. Demixing of the different-sized particles does occur in parts of the phase diagram, but elsewhere crystalline mixed structures form. Surprisingly, however, these binary alloy crystals frequently form in non-stoichiometric samples, with excess of one component phase-separated out of the crystalline regions. Moreover, the structures observed frequently do not match those expected from simple minimum volume considerations, and the time for the crystals to form can vary dramatically with sample composition, with many samples not crystallizing at all over observable timescales. This may reflect a kinetic effect resulting from a competition between crystallization and demixing. Thus, particular insight will be gained from studies of the kinetics of crystallization of binary mixtures; this will be fundamentally different than those of one-component suspensions given the requirement that both sizes must properly order into the mutual structure.

Studies of binary crystallization kinetics however, are severely hampered by the effects of sedimentation [11, 16], which are particularly problematic in mixtures of colloids because of the different effects for each type of particle, and the comparatively long evolution time of the structures. This has precluded study of the undisturbed kinetics of binary alloy colloidal crystals. In this paper, we study the crystallization of these structures through experiments performed on the International Space Station using the Physics of Colloids in Space apparatus [17], eliminating the effects of gravity; this allows us to accurately investigate the underlying kinetics of the crystallization. We see an extended induction time followed by relatively rapid crystallization. At long times, which are inaccessible in any ground-based experiment, anomalous slow ripening is seen. These alterations in the crystallization kinetics are likely a result of the effects of stoi-

chiometry, and provide new insight into the unexplained behavior of colloidal binary alloys.

We use samples consisting of poly-methyl-methacrylate (PMMA) spheres with a steric layer of poly-12-hydroxy-stearic acid, suspended in an index-matching mixture of decalin and tetralin; these particles have been shown to behave as nearly ideal hard spheres [2]. The particles were sufficiently monodisperse that they crystallized individually within 24 hours. To explore a range of variability of the binary alloys, we investigate two distinct crystal structures.

The first sample ( $R_A = 325$  nm,  $R_B = 130$  nm,  $\phi_A = 0.417$ ,  $\phi_B = 0.125$ , where  $R$  represents particle radius and  $\phi$  volume fraction) crystallized in a heretofore unreported structure, body-centered cubic (BCC)  $AB_6$ . This structure was discovered in the course of an extensive search for new binary structures at radius ratios less than 0.41 [14]. Apparently stable  $AB_6$  BCC is observed for size ratios 0.39 and 0.40, with number ratios around 5 B particles per A particle. It consists of a BCC arrangement of large particles with the small particles forming squares on each face of the unit cell. A model of this structure observed from the 100 and 110 faces is shown in figure 1a. Compared to previously known binary colloidal crystals such as  $AB_2$  and  $AB_{13}$  [11, 13], BCC  $AB_6$  can have a remarkably fast growth rate [14]. Large crystals, several millimeters in size, can, in some regions of its phase space, be formed within one day. To observe  $AB_6$  crystallite morphology, a sample was flown aboard the STS-95 Space Shuttle flight in 1998. White light photographs were taken of the crystals about one day after mixing. Large crystallites, 2-3mm in size, were observed and exhibited remarkably strong Bragg reflections. While some of the larger crystallites showed evidence of dendritic growth, intermediate size crystals appeared regular and smooth (Fig. 1b). Studied on earth, the same sample showed similar rapid crystallization, but exhibited smaller crystallites, presumably due to sedimentation.

To confirm the structure, a similar sample was made with larger PMMA particles which were dyed with two different colors and suspended in an index and near-density matching mixture of cycloheptyl bromide and decalin for observation with confocal microscopy [18]. The density matching solvent mitigates some effects of sedimentation, but also reduces the hardness of the interaction potential. This softening of the interaction potential would be expected to affect the structure and kinetics of the resulting phases [19, 20]. With this system, we were able to reproduce the phases seen in the hard-sphere systems, but the sample crystallized in less than a day, despite the significantly larger size of the particles, which may be an indication of the effects of the charging. Confocal microscope images of this sample show dramatically the marked ordering among the large particles in the  $AB_6$  crystals. Single domain crystals as large as 200-500 microns are common, and stacks of images in the vertical

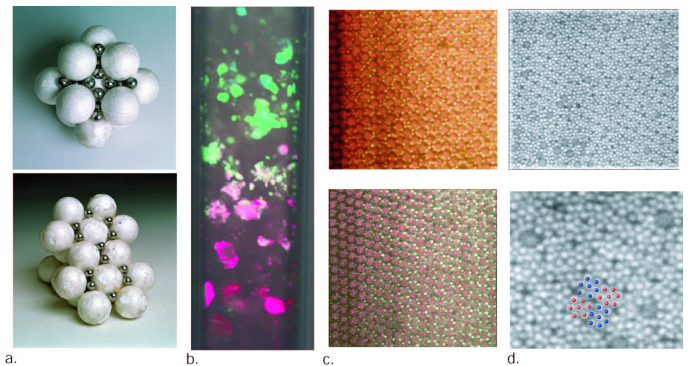


FIG. 1: a. Ball models of the 100 (top) and 110 (bottom) faces of an  $AB_6$  BCC crystal. b. Space grown  $AB_6$  BCC crystals. c. False color confocal images of the 100 and 110 faces of an  $AB_6$  BCC crystal ( $R_A = 825$  nm,  $R_B = 320$  nm) in a density-matched sample on earth. d. Confocal slice through the  $AB_{13}$  structure ( $R_A = 450$  nm,  $R_B = 258$  nm) along the centerplane of the 100 direction (see [11] for a model of  $AB_{13}$ ). The bottom panel shows a blow-up with colored spheres demonstrating the superlattice rotation of the icosahedra as described in the text.

direction show a high degree of three-dimensional ordering. False-color examples of such images are shown in figure 1c.

The second sample was made with radius ratio of 0.573 ( $R_A = 415$  nm,  $R_B = 238$  nm) and number ratio of around 19 small particles per large particle ( $\phi_A = 0.115$ ,  $\phi_B = 0.4105$ ). This sample crystallized in the  $AB_{13}$  structure, which exhibits a remarkably complex unit cell consisting of 112 particles [11, 13, 21]. It is a stable phase [22], despite the fact that the maximum packing fraction is significantly smaller than that of the phase-separated components. It is the most complex hard-sphere binary structure observed to date, consisting of a simple cubic lattice of large spheres surrounding icosahedra of small spheres. The icosahedra have edges towards the faces of the cubic unit cell, and neighboring icosahedra orient these edges perpendicularly to one another, forming a superlattice with a unit cell doubled in all directions from the basic cubic unit of the large particles. Confocal microscope images of an  $AB_{13}$  sample show smaller crystals and a higher prevalence of defects than the  $AB_6$  sample, but still allow the first three-dimensional in situ observation of this amazingly complicated crystal structure, including the superlattice ordering of the icosahedra (Fig.1d).

On the International Space Station, the samples are initiated into a disordered state through oscillatory rotational shear melting [8, 17]. Immediately after shear melting, the angular dependence of the light scattering from the samples shows only small broad fluid peaks. At long times after a mix, static scattering from both samples ("powder" diffraction patterns from the polycrystalline samples) shows strong, narrow crystalline peaks.

The  $AB_6$  scattering indexes to a body centered cubic (BCC) lattice (Fig. 2a), with no indications of coexistence with other structures. The  $AB_{13}$  peaks agree with observations of the scattering from isostructural crystalline  $NaZn_{13}$  [23], including the superlattice peaks that indicate the doubling of the unit cell (Fig. 2b). The asymmetric appearance of nearby Bragg peaks at early times indicates that the superlattice peaks may be present in the development of the initial structure, although they are not fully resolved until much later as the peaks narrow. The significant increase in both the strength and sharpness of the peaks in these samples by comparison to those observed in one-component systems illustrate a fundamental difference between the structures of these binaries and the one-component crystals. The  $AB_6$  and  $AB_{13}$  structures are both perfect, three-dimensionally ordered crystals leading to sharp, intense Bragg peaks, whereas one-component crystals form stacks of two-dimensional layers with lateral disorder (random hexagonal close packing) [2, 8], leading to broad rods of scattering as well as Bragg peaks. Indeed, the lowest order Bragg peaks of the  $AB_6$  crystal are among the most intense and sharpest such peaks observed for untemplated colloidal crystals.

In order to gain understanding of how the crystallization evolves after mixing in these samples, we follow the development of the strongest Bragg peaks as a function of time after initiation. From the integrated intensity of a peak, we can deduce how the total amount of crystal is changing, and from the half width at half maximum of the peaks, we can extract the average extent of the crystallized regions [3].

Results for the  $AB_{13}$  sample show the timescale for crystallization of this sample to be on the order of 100 hours, with a distinctly non-power-law evolution with time (Fig. 3a). For the first 50 hours after initialization, no peaks are visible above the scattering background. At around 50 hrs, the first peak appears and at around 100 hours, the next two reflections at higher scattering vector  $Q$  also become visible. During the time from 50 to 100 hours, the first peak shows significant narrowing, reflecting a rapid growth of crystalline regions. After 100 hours, however, the growth levels off. From 100 hours until the latest time measured, the crystallite growth of the 220 peak crosses over to an apparent power law with an exponent close to 0.25. This is significantly slower than the power laws predicted by models of ripening, in which large crystals grow at the expense of smaller crystals. A system with a non-conserved order parameter like crystallinity (which is non-conserved because the total amount of crystallinity in the system can vary with time) should follow Lifshitz-Allen-Cahn [24] ripening, which predicts an exponent of 0.5, while Lifshitz-Slyozov [25] ripening, which holds for a conserved order parameter (such as particle density, which cannot change in one part of the sample without a compensating change

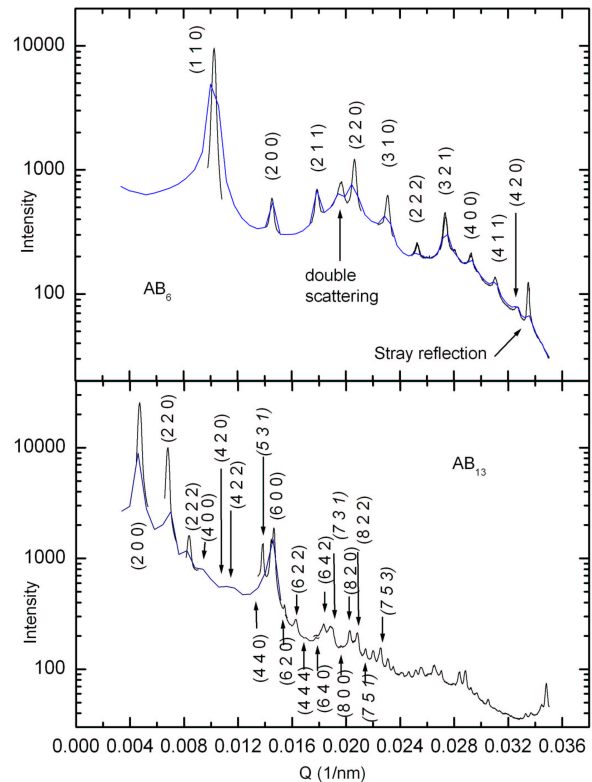


FIG. 2: Long-term light scattering "powder" diffraction patterns from the polycrystalline samples. Measurements at different times are spliced together. The top panel shows  $AB_6$  BCC, the bottom panel is  $AB_{13}$  with odd-numbered reflections (in italics) indicating superlattice reflections.

in another part of the sample), predicts an exponent of 0.33. For colloids, crystallization is accompanied by a change in local density, and these two order parameters are therefore coupled, so it is unclear which ripening behavior should be observed; yet the exponent we see is measurably smaller than either. For the same region of time, the growth of the area under the peaks also shows a significant slowing down. However, even at the latest time measured, several months after mixing of the sample, new area is still being added to the peaks, which indicates that small amounts of new crystal are slowly being developed in the system, and hence it is not in a true ripening regime, where no new crystal should be formed. One qualitative explanation for this is that as crystal forms, the populations of the small and large particles in the remaining fluid phase change relative to one another. This alteration of the 'melt' composition would be expected to affect the growth rate, and perhaps lead to a continual slowing of the formation of new crystal.

Results for the peak widths of the  $AB_6$  sample give similar results to those found in  $AB_{13}$ . In contrast to

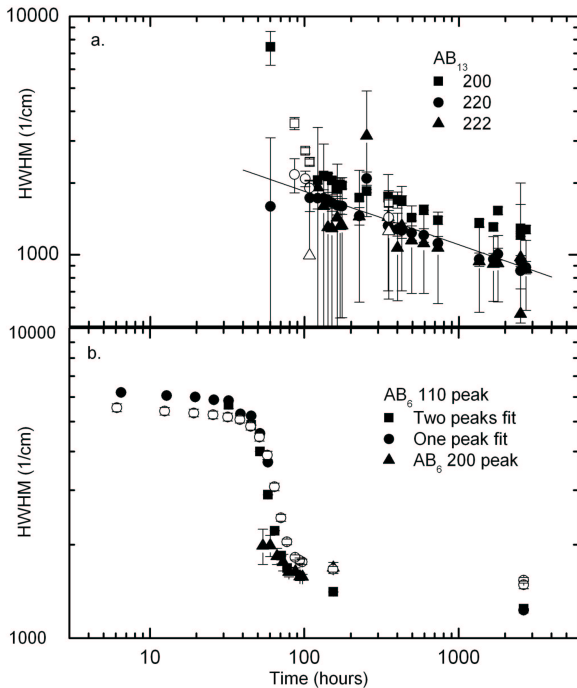


FIG. 3: Half width at half maximum of Bragg peaks in the two binary samples. For AB<sub>6</sub>, most of the data are from fiber scattering, open symbols are from a fluorescing screen. For AB<sub>13</sub>, data from the first three Bragg peaks are shown.

AB<sub>13</sub>, however, the fluid peak in the AB<sub>6</sub> sample sits very near the first Bragg peak, making it difficult to extract reliable information about the integrated peak intensity. We did not have sufficient resolution to determine whether the observed peak development was the result of evolution of the fluid peak toward a crystalline peak, or the addition of a crystalline peak on top of a decreasing fluid peak. However, the width is relatively insensitive to the exact fitting function, as can be seen from the overlap of the one and two-peak fits in figure 3b. For the first 40 hours, the width changes only very slowly. After this time, the observed peak narrows rapidly, faster even than the peaks in AB<sub>13</sub>, though some of this is likely an artifact due to the combined evolution of the fluid and crystal peaks. Slower growth is seen for the 200 peak, though this peak is not visible until the crossover near the end of the fast growth period. Beyond around 70 or 80 hours, the development slows down, and any ripening seen is much slower even than that in the AB<sub>13</sub> sample.

Comparison of the scattering for binary mixtures with that of one-component samples indicates intriguing differences. One-component samples show a delay before

the onset of crystallization [3], which has been characterized using an 'induction' time scale in addition to the usual nucleation time. However, the minimum induction times seen for the binary samples are generally much longer than the minimum times for the one-component samples. This is likely due to: a large-scale rearrangement of the component particles of the sample that allows stoichiometric crystallization to proceed, competition between different phase behaviors, or possibly nucleation centers are forming, and statistically the critical nucleation size is not reached for a long time due to high surface tension or low bulk chemical potential difference. At long times, the anomalous slow ripening also indicates fundamental differences between the evolution of the binary samples and that of the one-component systems. This ripening may be driven by the changing of particle number ratios in the coexisting fluid, which does not occur for single component systems. Moreover, the slow development of the crystallization highlights the possibility that the lowest energy structures may not be achieved with some binary colloidal crystals because of the very slow evolution of the ordered structures. These observations represent the first study of undisturbed crystallization kinetics in binary colloidal suspensions and should serve as an experimental benchmark against which to compare the results of theory, simulation, and ground-based experiments with near-density matching or tumbling to time-average out gravitational effects.

We gratefully acknowledge support from NASA (NAG3-2284).

- 
- [1] W. G. Hoover and F. H. Ree, *Journal of Chemical Physics* **49**, 3609 (1968).
  - [2] P. N. Pusey and W. v. Meegen, *Nature* **320**, 340 (1986).
  - [3] J. L. Harland and W. v. Meegen, *Physical Review E* **55**, 3054 (1997).
  - [4] S. Auer and D. Frenkel, *Nature* **409**, 1020 (2001).
  - [5] U. Gasser, E. R. Weeks, A. Schofield, P. N. Pusey, and D. A. Weitz, *Science* **292**, 258 (2001).
  - [6] T. Palberg, *Journal of Physics: Condensed Matter* **11**, R323 (1999).
  - [7] K. Schatzel and B. J. Ackerson, *Physical Review E* **48**, 3766 (1993).
  - [8] J. X. Zhu, M. Li, R. Rogers, W. Meyer, R. H. Ottewill, W. B. Russel, and P. M. Chaikin, *Nature* **387**, 883 (1997).
  - [9] V. L. Colvin, *MRS Bulletin* **26**, 637 (2001).
  - [10] D. Frenkel and A. A. Louis, *Physical Review Letters* **68**, 3363 (1992).
  - [11] P. Bartlett, R. H. Ottewill, and P. N. Pusey, *Physical Review Letters* **68**, 3801 (1992).
  - [12] M. D. Eldridge, P. A. Madden, and D. Frenkel, *Nature* **365**, 35 (1993).
  - [13] N. Hunt, R. Jardine, and P. Bartlett, *Physical Review E* **62**, 900 (2000).
  - [14] A. B. Schofield, P. Ratcliffe, and P. N. Pusey (to be pub-

- lished).
- [15] A. B. Schofield, *Physical Review E* **64**, 051403 (2001).
  - [16] P. Bartlett and R. H. Ottewill, *Advances in Colloid and Interface Science* **50**, 39 (1994).
  - [17] R. R. Ansari, E. A. Hovenac, S.Sankaran, J. M. Koudelka, D. A. Weitz, L. Cipelletti, and P. N. Segre, *Space Technology and Applications International Forum STAIF-99* (1999).
  - [18] We estimate the buoyancy mismatch to be of order  $10^{-3}$ , low enough to limit sedimentation in the small microscope cell, but not sufficiently low to eliminate sedimentation of larger crystallites formed in the bigger cell volume.
  - [19] J. M. Mendez-Alcaraz, M. Chavez-Paez, B. D'Aguanno, and R. Klein, *Physica A* **220**, 173 (1995).
  - [20] R. Garibay-Alonso, J. M. Mendez-Alcaraz, and R. Klein, *Physica A* **235**, 159 (1997).
  - [21] J. V. Sanders, *Philosophical Magazine A* **42**, 705 (1980).
  - [22] M. D. Eldridge, P. A. Madden, P. N. Pusey, and P. Bartlett, *Molecular Physics* **84**, 395 (1995).
  - [23] D. P. Shoemaker, R. E. Marsh, F. J. Ewing, and L. Pauling, *Acta Crystallographica* **5**, 637 (1952).
  - [24] S. M. Allen and J. W. Cahn, *Acta Metallurgica* **27**, 1085 (1979).
  - [25] I. M. Lifshitz and V. V. Slyozov, *J. Phys. Chem. Solids* **19**, 35 (1961).



# Spinodal decomposition in a model colloid-polymer mixture in microgravity

A.E. Bailey,<sup>1,\*</sup> W. C. K. Poon,<sup>2</sup> R.J. Christianson,<sup>1</sup> A. B. Schofield,<sup>2</sup> U. Gasser,<sup>1,†</sup> V. Prasad,<sup>1,‡</sup>  
S. Manley,<sup>1</sup> P.N. Segre,<sup>1,§</sup> L. Cipelletti,<sup>1,¶</sup> M.P. Doherty,<sup>3</sup> S. Sankaran,<sup>3</sup> A.L. Jankovsky,<sup>3</sup>  
B. Shiley,<sup>4</sup> J. Bowen,<sup>4</sup> J. Eggers,<sup>4</sup> C. Kurta,<sup>4</sup> T. Lorik,<sup>4</sup> P. N. Pusey,<sup>2</sup> and D. A. Weitz<sup>1</sup>

<sup>1</sup>*Dept. of Physics & DEAS, Harvard University, Cambridge, MA 02138*

<sup>2</sup>*School of Physics, The University of Edinburgh, Mayfield Road, Edinburgh EH9 3JZ, Scotland*

<sup>3</sup>*NASA Glenn Research Center, Brook Park, OH 44135*

<sup>4</sup>*Zin Technologies, Inc., Brook Park, OH, 44142*

(Dated: May 11, 2004)

We studied spinodal decomposition in a mixture of hard-sphere colloids and non-adsorbing, nearly-ideal linear polymers in microgravity using small-angle light scattering and direct imaging. During the experiment, we observed a clear crossover from early-stage, diffusion-limited spinodal decomposition to late-stage, interfacial-tension driven coarsening. Data acquired over 5 orders of magnitude in time show more than three orders of magnitude increase in domain size. In dimensionless units, the domain size evolves along nearly the same path as that measured in binary liquid mixtures. The late stage growth is found to approach the expected linear growth rate quite slowly.

PACS numbers: 64.75.+g,82.70.Dd,64.70.-p

The kinetics of phase separation in colloid-polymer mixtures could be expected to be quite different from the same process in process in binary liquids. Spinodal decomposition occurs in the colloid-polymer (C-P) mixtures in which the range of the depletion interaction exceeds a critical dimensionless value[1],  $\tilde{r} = r_g/R$  where  $r_g$  is the polymer radius of gyration and  $R$  is the colloid radius. During phase separation the colloidal particles must diffuse through a fluid of polymer suspended in a solvent, while the polymer must simultaneously reappportion to maintain a constant osmotic pressure throughout the sample. Spinodal decomposition in binary liquids proceeds via the rapid growth of thermal concentration fluctuations whose wavelengths are longer than a critical wavelength proportional to the correlation length. A C-P mixture far from its critical point will have no such fluctuations because the correlation length cannot be smaller than the colloid size. In practice, the correlation length of liquid mixtures can only reach the size of moderately large colloids close to the critical consolute point, where composition fluctuations diverge in amplitude as well as size. Dhont's first-principles calculations [2] recovered many aspects of the 'classical' picture for simple fluids [3, 4], but also pointed to the possibility of subtle new features specific to colloids.

The properties of colloidal gas and liquid phases in c-p mixtures and the phase separation process itself have been the subject of several studies. Two groups have measured, the interfacial tension,  $\gamma$  [5–7]. Both the order-parameter and correlation length critical exponents,  $\beta$  and  $\nu$ , were found to have Ising values [8]. Phase separation experiments[9] using very small colloids measured domain growth consistent with early stage phase separation, but gravity limited the available time-window. Gravity-driven sedimentation severely limits the study of phase separation in colloidal systems on Earth because

both the denser phase and the colloids within each phase sediment. Gravity also drives convective mixing in the presence of temperature gradients. Thus, evolution of the phase separation process in C-P mixtures remains largely unexplored.

In this letter, we report an experimental study of spinodal decomposition and coarsening in gas-liquid coexistence in a model c-p mixture in the microgravity environment of the International Space Station. The dynamics of the phase transition are remarkably similar to those measured in binary liquids in proximity to their critical consolute point.

NASA's 'Physics of Colloids in Space' instrumentation [10] permits simultaneous light scattering and direct observation. The cylindrical sample cells are 20 mm in diameter by 10 mm in height. A window in the bottom of the cell allows the sample to be imaged using two digital color cameras having different spatial resolutions: approximately 4.4  $\mu\text{m}$  and 44  $\mu\text{m}$ . Small-angle scattering from an 8 mm diameter, 533 nm laser beam is collected by a CCD camera imaging the focal plane of a 103 mm focal length lens comprising the top of the sample cell, collecting scattered light from scattering angles of 0.1° to 6.0°. Small angle scattering can be measured as fast as 0.33 Hz and color images acquired as quickly as 1 Hz. Additional optics allowed static light scattering over a range of 11° to 169° scattering angle. The phase-separated sample could be homogenized in-situ with oscillatory shear. The experiment was launched on mission STS-100 aboard NASA Shuttle *Endeavor* and was operated aboard the International Space Station for more than eight months remotely from the NASA Glenn Research Center.

Polymethylmethacrylate (PMMA) particles with  $R = 159$  nm (from static light scattering) were synthesized using standard procedures [11]. Polystyrene with  $M_w = 13.2 \times 10^6$  was purchased from Polymer Laboratory. A

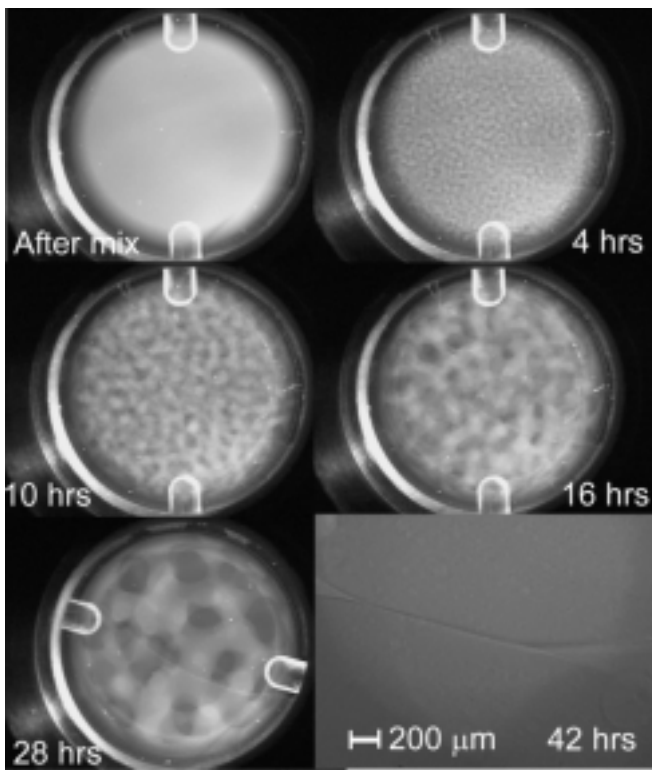


FIG. 1: Images of a colloid-polymer mixture undergoing spinodal decomposition in microgravity. The time after homogenization is shown in each image. The five images covering the time from immediately after the mix to 28 hrs after the mix show the entire 2 cm diameter sample cell. The bottom right image shows a higher resolution view of an interface between domains in the sample cell.

60:40 (by volume) mixture of cis-decalin and tetralin was used to partially match the refractive index of the particles. In this mixture, the polymer has an estimated  $r_g = 101$  nm [12], so that  $\tilde{r} = 0.63$ . The sample had a colloid volume fraction  $\phi = 0.22$  and polymer concentration  $c_p = 1.285$  mg/ml. On earth, it phase separated completely over  $\gtrsim 2$  hours into 45%:55% colloidal liquid and gas phases.

After each mix the sample progressed from an initially homogeneous state to one in which an interconnected domain structure coarsened. Fig. 1 shows a series of five images taken at various times during the phase separation process. The domains appear undisturbed by the presence of the cell walls up to approximately 42 hours after mixing. After this time, the domain pattern distorts and the colloid-rich phase collapses to one side of the sample cell. The colloid-rich phase coats the surfaces of the cell approximately 60 hours after mixing. Static light scattering, performed when the colloid-rich phase occupied the scattering volume, showed a liquid structure factor. An equivalent measurement performed on the colloid-poor phase reveals only the particle form factor without interparticle correlation.

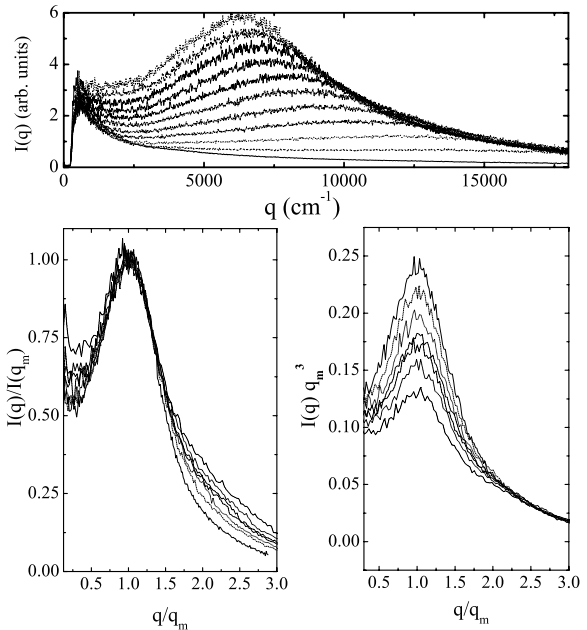


FIG. 2: Raw data and two forms of scaling. The upper portion shows raw SALS data exhibiting growth of fluctuations and length scale typical of spinodal decomposition. From bottom to top, the times after the mixing quench are 2, 6, 10, 13, 17, 21, 25, 28, 32, 36, and 40 seconds. The left graph shows scaling of SALS data scaled the peak height and plotted against the wave vector scaled by the peak position. The right-hand graph is a test of dynamic scaling over the same range of time, 85 - 188 sec after the sample is quenched.

The colloid volume fraction of the separated phases can be estimated from static light scattering results. The angular distribution of the scattering from the liquid phase is a combination of the colloid form factor multiplied by a liquid structure factor and the form factor for Gaussian polymer coils. Using an approximate analytic solution of the Percus-Yevik approximation[13] for the liquid structure factor, a fit of the data gives  $\phi_{\text{liquid}} = 0.477 \pm 0.002$ . Conservation of mass  $0.55 \times \phi_{\text{gas}} + 0.45 \times \phi_{\text{liquid}} = 0.22$  yields the volume fraction of the liquid phase  $\phi_{\text{gas}} = 0.010$ .

Immediately after homogenization, the sample undergoes spinodal decomposition. The top of Fig. 2 shows typical small angle light scattering (SALS) results. Two seconds after mixing no increase in fluctuation amplitude is observed. The next curve, 6 s after mixing, shows an increase in fluctuations at all accessible  $q$ . Another 4 s later, a peak is observed, which shifts to lower  $q$  as time progresses. Stray light appears as a sharp peak at the smallest  $q$  at these early times. Because the particle form factor varies by only 1.8% over this  $q$  range, the scattered intensity is an accurate measurement of the time-dependent structure factor  $S(q, t)$ , where  $t$  is the

time after quench.

Our SALS data satisfies self-similarity scaling[15]. Self-similarity scaling is shown in the left graph of Fig. 2, plotting  $S(q, t)/S(q_m, t)$  vs.  $q/q_m$  where  $q_m$  is the position of the peak in  $S(q)$  at time  $t$  after homogenization. This scaling demonstrates that the shape of the peak is time invariant. As the dominant length scale increases, the width of the fluctuation spectrum decreases. The data have not been corrected for stray light or multiple scattering. The latter accounts for the slight increase in scattering in the vicinity of  $q/q_m = 2$ , due to double scattering of light from the main (singly-scattered) SALS peak[14].

Dynamic scaling[2, 15] results from the assertion that all physical parameters of the coarsening system scale with dominant length scale. A test of dynamic scaling is shown right-hand graph of Fig. 2 as  $S(q, t)q_m^3 / \int_0^\infty q^2 S(q, t) dq$  vs  $q/q_m$ . The integral normalization has been shown theoretically[2] and experimentally[9] necessary in systems where hydrodynamics are important. Furukawa's scaling approach applies to the later stages of phase separation where well formed domains or droplets are growing and  $S(q_m, t) \sim q_m^{-d}$ , where  $d$  is the dimensionality. The scattering data shown here is acquired during the early, diffusion-limited stage of spinodal decomposition; hence, this scaling does not apply. During the time regime shown,  $q_m \sim t^{-1/2}$ ,  $S(q_m) \sim t$  and the normalization is nearly constant.

The dominant length scale in the system at any time,  $\ell(t)$ , is related to the SALS peak position by  $\ell(t) = 2\pi/q_m(t)$ . When this length scale becomes so large that  $q_m$  can no longer be resolved with SALS,  $\ell(t)$  can be obtained by analyzing the real-space images. The 2-D correlation function,  $C(r) = \langle I(\vec{r})I(\vec{r} - \vec{r}_0) \rangle / \langle I(\vec{r})^2 \rangle$ , was computed numerically by multiplying an image by a copy of itself that was shifted by an offset  $\vec{r}_0$  from an arbitrary origin. The normalization fixed the value at zero offset to unity. The lowest-order peak in the azimuthally-averaged  $C(r)$  was fit locally to a Gaussian to obtain the position taken as  $\ell(t)$ . This was converted to an equivalent SALS peak position using  $q_m = 2\pi/\ell$ .

Growth of the domain size follows a crossover from diffusion-limited dynamics to interfacial-tension driven dynamics. If phase separation is occurs exclusively by diffusion,  $q_m \sim t^{-1/3}$  is expected [16], which is consistent with the first few data points shown in Fig. 3. The peak position quickly begins to move more rapidly with time. At later times, domains coarsen by interfacial-tension-driven viscous flow [16]. Different regions of the bi-continuous structure (cf. Fig. 1) have different radii of curvature,  $r$ , and therefore different Laplace pressures,  $\sim \gamma/r$ . The resulting Poiseuille flow drives the coarsening of regions with large  $r$  at the expense of those with

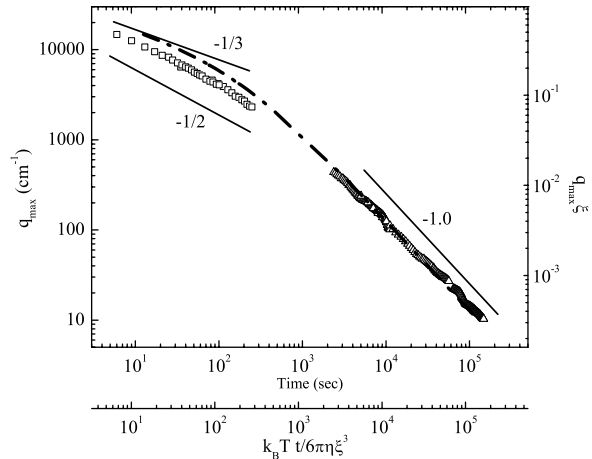


FIG. 3: The reciprocal-space peak position as a function of time,  $q_m(t)$  on a double-log plot. Short-time data from SALS, and long-time data from direct imaging. The lines have slopes  $-1/3$ ,  $-1/2$  and  $-1$  as indicated. The dash-dot line is the evolution of the domain size in binary liquids plotted relative to the dimensionless axes. The upper x-axis is time in seconds while the lower x-axis is the scaled time time described in the text. For this sample, they differ by only 12%.

small  $r$ . Siggia has shown that this mechanism leads to

$$\ell(t) \sim \left(\frac{\gamma}{\eta}\right) t^1, \quad (1)$$

where  $\eta$  is the viscosity of the coarsening phase[16]. Examining the difference between the data and a  $t^1$  growth law reveals that this this exponent is reached at approximately  $3 \times 10^4$  s after the homogenization. Prior to this time, the exponent is slightly less than 1.0. Dhont has shown that the growth exponent can vary between 0.2-1.1 depending on the importance of hydrodynamic interactions [2] during the the intermediate stages of growth. Because this stage is characterized by local density variations which are not small and diffuse interfaces between the domain, this regime has a very short duration. SALS data exhibit a  $I \sim q^{-4}$  consistent with scattering from sharp interfaces as early as 85 s after homogenization.

During the early-stage, diffusive period of phase separation, the dynamics of the process are controlled by a single, time-independent length scale, the correlation length  $\xi$ . Siggia argues that the cross-over from diffusive dynamics to late stage dynamics occurs at  $q_m \xi \sim 0.1$ . Extrapolating forward in time from the early stage points with  $q_m \sim t^{-1/3}$  and backward from the late stage points with  $q_m \sim t^{-1.0}$ , the two intersect at  $q_m = 3350 \text{ cm}^{-1}$ . Applying Siggia's result for the crossover,  $\xi = 300 \text{ nm}$  which is only 6% smaller than colloid diameter. Given the uncertainty in this estimation, it is reasonable to assume  $\xi = 2R$ .

Using this value, the time evolution of the dimensionless domain size can be compared with that measured during spinodal decomposition of binary liquids. The results of several studies of phase separation of critical mixtures of simple liquids collapses to a single curve when the evolution is graphed in terms of dimensionless quantities [17]. The maximum wave vector is reduced by the correlation length as  $q_m\xi$ , and the time is reduced by the relaxation time of a fluctuation with wave vector  $1/\xi$ ,  $\tau = k_B T t / (6\pi\eta\xi^3)$ . Using the correlation length deduced above, the length and time axes of Fig. 3 were rescaled as shown. The continuous curve shown in the figure is a result from Guenoun et al. This result is a fit of data collected from isodensity binary fluid to a form derived by Furukawa. This simple function accurately captures the physical scaling at both early and late stages and assumes a smooth crossover between. The evolution of the dominate length scale in the c-p sample is very comparable to that of binary liquids. The c-p system has a longer length scale at early time and a more gradual crossover to interfacial tension driven coarsening.

The late stage growth rate is consistent with the interfacial tension estimated by

$$\gamma = \frac{nk_B T \phi}{\xi^2} \quad (2)$$

where  $nk_B T$  is the strength of the interaction between the colloidal particles induced by the presence of the polymer. Using the interaction derived by Asakura and Oosawa [18, 19],  $n = 2.65$ . This value results in an estimate of the interfacial tension of  $2.4 \times 10^{-8}$  N/m. During the late stages of phase separation, the domain size should vary as  $L \sim (\lambda\gamma/\eta)t$ , where  $\lambda$  is a dimensionless coupling constant between the the order parameter and the fluid flow velocity[16, 20]. Siggia estimated  $\lambda \sim 0.01$  based on scaling arguments. Later San Miguel et al. derived a value of 0.04. Experimentally, Guenoun et al. have found 0.011 appropriate for all binary liquid data. Fitting our late stage data to a linear growth law results in a growth rate of  $4.1 \times 10^{-8}$  m/s, which implies  $\lambda = 0.01$ . Thus, the rate of late stage growth is completely consistent with the interfacial tension estimated from the properties of the sample and the coupling constant agrees with that deduced from binary liquids.

The quench conditions of the c-p mixture studied here are comparable to those of critical binary liquid mixtures. The interfacial tension measured in this study,  $2.4 \times 10^{-8}$  Nm<sup>-1</sup> is equal to that of a critical mixture of cyclohexane and methanol 1.25 mK from the critical point[21]. Because the basic dimension is that of the colloids, samples do not need to be made in proximity to the critical point to obtain such small interfacial tensions. The correlation length of the cyclohexane methanol mixture at the same distance from the critical temperature would be 415 nm[22], which is very comparable to the 320 nm estimated in the c-p mixture presented here.

The microgravity conditions of this experiment are essential. A density mismatch of the order of 1 part per thousand between the particles and the solvent leads to sedimentation overtaking interfacial growth at the point of the diffusive-viscous cross over in space. Obtaining and maintaining (e.g. against temperature fluctuations) this degree of density matching on earth is non-trivial. On the other hand, a 1 in  $10^{-3}$  density mismatch is equivalent to performing experiments on non-density-matched samples in a gravity of  $10^{-2}g$ . The International Space Station achieves residual accelerations four orders of magnitudes below this figure [23].

According to recent simulations [4], the viscous regime should cross over to an inertial regime, where the demixing-driven flow becomes turbulent, when domains grow to  $\ell = \eta^2 / (\rho\gamma)$ , where  $\rho$  is the average mass density of the fluid system. For our system, this requires  $\sim 1.5$  m domains, the large size basically reflecting the low surface tension involved. This figure reduces to  $\sim 1$  mm for a system with  $\sim 10$  nm particles far from criticality, which may then be usable for studying the inertial regime.

In addition to the possibility of studying small colloids in an attempt to observe inertial regime of phase separation, the other extreme of larger colloids and closer proximity to the critical point could yield unprecedentedly low interfacial tension and phase separation on time scales never before observed in simple systems.

This work was supported by NASA(NAG3-2284).

- 
- \* Current Address: Scitech Instruments, Inc., North Vancouver, BC, Canada V7J 2S5
  - † Current Address: Dept. of Physics, University of Konstanz, Konstanz, Germany
  - ‡ Current Address: Dept. of Chemical Engineering, UCSB, Santa Barbara, CA
  - § Current Address: NASA Marshall SpaceFlight Center, Huntsville, Al 35812
  - ¶ Current Address: GDFC cc 26, Universite Montpellier II, P. E. Bataillon, Montpellier 34000, France
- [1] W. C. K. Poon, J. Phys. Condens. Matter **14**, R859 (2002).
  - [2] J. K. G. Dhont J. Chem. Phys. **105**, 5112 (1996).
  - [3] P. M. Chaikin and T. C. Lubensky, *Principles of Condensed Matter Physics* (Cambridge: Cambridge University Press 1995), Section 8.7.
  - [4] V.M. Kendon, M.E. Cates, I Pagonabarraga, J.-C. Desplat and P. Blandon, J. Fluid Mech. **440**, 147 (2001).
  - [5] E.H.A. de Hoog and H.N.W. Lekkerkerker, J. Phys. Chem. B **103**, 5274 (1999).
  - [6] E. H. A. de Hoog, H. N. W. Lekkerkerker, J. Schulz, and G. H. Findenegg J. Phys. Chem. B **103**, 10657 (1999).
  - [7] B.-H. Chen, B. Payandeh, and M. Robert, Phys. Rev. E **62**, 2369 (2000).
  - [8] B.-H. Chen, B. Payandeh, and M. Robert, Phys. Rev. E **64**, 042401 (2001).

- [9] N.A.M. Verhaegh, J.S. van Duijneveldt, J.K.G. Dhont, and N.H.W. Lekkerkerker *Physica A* **230**, 409 (1996).
- [10] C. T. Lant, A. E. Smart, D. S. Cannell, W. V. Meyer and M. P. Doherty, *Appl. Optics* **36**, 7501 (1997).
- [11] J. W. Antl et al. *Colloid Surf.* **17**, 67-78 (1986).
- [12] V. Prasad, unpublished Ph.D. dissertation, Harvard University (2002).
- [13] L. Verlet and J.-J. Weis, *Phys. Rev. A* **5**, 939 (1972).
- [14] A. E. Bailey and D. S. Cannell, *Phys. Rev. E* **50**, 4853 (1994).
- [15] Furukawa *Adv. Phys.* **34**, 703 (1985).
- [16] E. D. Siggia *Phys. Rev. A* **20**, 393 (1979).
- [17] P. Guenoun, R. Gastaud, F. Perrot, and D. Beysens, *Phys. Rev. A* **36**, 4876 (1987).
- [18] S. Asakura and F. Oosawa, *J. Polymer Sci.* **33**, 193 (1958).
- [19] A. Vrij, *Pure Appl. Chem.* **48**, 471 (1976).
- [20] T. Lookman, Y. Wu, F. J. Alexander, and S. Chen, *Phys. Rev. E* **53**, 5513 (1996).
- [21] C. Warren and W. W. Webb, *J. Chem. Phys.* **50**, 3694 (1969).
- [22] C. Houessou, P. Guenoun, R. Gastaud, F. Perrot, and D. Beysens, *Phys. Rev. A* **32**, 1818 (1985).
- [23] K. Jules, K. McPherson, H. Hrovat, E. Kelly, IAC-02-J.6/T.5.02, 53rd International Astronautical Congress, 2002.



# Physics of Colloids in Space (PCS)

*U.S. Principal Investigator:* **DAVID A. WEITZ**, Harvard University

*Co-Investigators:* **Peter Pusey**, University of Edinburgh UK

*Chief Scientist:* **Art Bailey**, Scitech Instruments, Inc.,

*Project Scientist:* **Subramanian Sankaran**, NCMRfc/NASA GRC

*Project Manager:* **Michael Doherty**, NASA GRC

(EXPPCS Postflight Report)

## I. INTRODUCTION

### Abstract

The Physics of Colloids in Space (PCS) experiment was accommodated within International Space Station (ISS) EXpedite the PRocessing of Experiments to Space Station (EXPRESS) Rack 2 and was remotely operated from early June 2001 until February 2002 from NASA Glenn Research Center's Telescience Support Center (TSC) in Cleveland, Ohio, and from the remote site at Harvard University in Cambridge, Massachusetts. PCS was launched on 4/19/2001 on Space Shuttle STS-100 (ISS Flight 6A.) The experiment was activated on 5/31/2001. The entire experimental setup performed remarkably well, and accomplished 2400 hours of science operations on-orbit.

The sophisticated instrumentation in PCS is capable of dynamic and static light scattering from 11 to 169 degrees, Bragg scattering over the range from 10 to 60 degrees, dynamic and static light scattering at low angles from 0.3 to 6.0 degrees, and color imaging. The long duration microgravity environment on the ISS facilitated extended studies on the growth and coarsening characteristics of binary crystals. The demixing of the colloid-polymer critical-point sample was also studied as it phase-separated into two phases. Further, aging studies on a col-pol gel, gelation rate studies in extremely low concentration fractal gels over several days, and studies on a glass sample, all provided valuable information.

These experiments have given us tremendous amount of fresh data and knowledge, and it is truly worthwhile to achieve further steady stream of valuable data beyond what we have amassed with these PCS samples so far. The hardware will be used for other upcoming investigations named PCS+ and PCS-3 that will study monodisperse crystals and glasses, binary samples similar to PCS, and binary glasses, and anisometric colloids that have rod-like particles.

PCS was managed by GRC.

### Hypothesis

The purpose of the Physics of Colloids in Space experiment, or PCS, is to study colloidal suspensions in the microgravity environment of International Space Station. Focus in PCS was on the physics of colloidal particles, including binary colloidal alloys, colloidal particles with depletion interactions, and large scale fractal aggregates and gels. The details of the nucleation, growth rate and morphology for all these classes of fluids in the absence of gravity are measured to compare with the theoretical predictions. Microgravity is required because most of the structures require extended periods of time to nucleate and grow, during which time sedimentation effects must be completely eliminated to ensure that the desired alloy structure is produced.

### Objectives

The objective of PCS is to address key problems in the physics of colloidal particles, including the nucleation, growth, and properties of binary colloidal alloys, the structure, stability, and equilibrium properties of colloidal particles with attractive interactions induced, in a controllable fashion, by adding polymers, and the structure, dynamics, and mechanical properties of large scale fractal aggregates. Quantitative data on nucleation and growth in the absence of gravity, for four classes of colloidal samples, namely, binary colloidal crystals, colpol mixtures, fractal gels, and a glass sample are of interest.

### Background/History

The PI and Co-I proposed *Colloidal Physics in Microgravity* in response to NRA 91-OSSA-17. The essence of this proposal is to study the formation of novel materials from three kinds of colloidal suspensions, and to explore their physical properties. The three kinds of colloidal suspensions are: binary colloidal alloys, colloid polymers, and fractal aggregates.

The binary colloidal alloys are made up of sub-micron PMMA spheres suspended in a liquid. The spheres are the same acrylic type particle used in monodisperse colloidal suspensions, but in the case of binary alloys, two different sized spheres are dispersed in the liquid. Under certain conditions, it has been found that binary dispersions at size ratio  $r=0.58$  form both the AB2 and the AB13 superlattice structures. AB2 consists of a simple hexagonal arrangement of large A particles, with the smaller B particles filling all the interstices between the A layers, while in AB13, icosahedral clusters of 13 small B particles are body centered in a simple cubic lattice of A particles. We believe that someday these binary colloidal systems may become useful in communications technologies as optical filters or displays. Colloidal polymers are similar to binary colloidal alloys but with spherical acrylic particles of one size and a chainlike polymer particle added to the colloidal suspension. Polymers are often added to colloids to control their properties and adjust their behavior. In paint, polymers control the way the paint spreads across a surface. We are studying these colloidal structures with the hope of learning how they form, how stable they are, and how strong they are. Fractal aggregates are structures formed from colloidal particles where the basic structural shape of any one part is similar to the structural shape of the whole object. A Christmas tree, a snowflake, or a fern are good examples of fractal structures. For the investigations with fractal aggregates, two types of colloidal particles are significant to study: polystyrene, and silica. Each is to be suspended in water and combined in-situ during the mission with a salt solution to form the fractal aggregate sample. All three colloidal systems are capable of being probed using visible light.

For our experiment opportunities on ISS, the objectives of the experiments are to develop the basic principles for synthesizing several different sorts of materials, to determine the fundamental properties of these materials, to fully develop the evolving field of "colloid engineering", and to create materials with novel properties using colloidal particles as the precursors. Our objectives are being addressed in two steps. First, the determination of the fundamental structures, dynamics, and properties of the three kinds of colloid suspensions will be conducted using the PHaSE-heritage light scattering instrument, the Physics of Colloids in Space Apparatus. This is the present experiment on ISS - the Experiment on Physics of Colloids in Space (EXPPCS).

Second, the creation and evaluation of materials with novel properties by using the first step findings and by using new materials requires the particle level characterization capabilities intended for the microscope-based Light Microscopy Module. This

future experiment is planned to be performed in the GRC Fluids Integrated Rack (FIR).

## II. METHODS/RESEARCH OPERATIONS

### Functional Objectives

PCS contains a total of eight approximately 3 milliliter volume colloid samples, each contained by a glass cell stationed within a remotely controlled carousel inside the PCS Test Section. Initiation of an investigation on each colloid sample occurs when it is homogenized (that is, stirred up via the oscillation of the sample cell within its bearings) to evenly distribute its suspended particles and then allowed to sit for days, weeks, or months on orbit. During this interval, particles in the samples will organize themselves - that is, self-assemble - into crystal-like or gel-like arrangements. Meanwhile, the laser light scattering and visual imaging diagnostics are utilized to gather structural information about the samples during this crystallization or gelation process. All samples, except the two fractal gels, can be rehomogenized (reinitiated) to repeat a measurement at another sampling rate or to utilize a different measurement technique to examine their behavior in a complementary way. The fractal gels can only be run once. For all samples, measurements are taken every few seconds immediately after homogenization and then with less frequency (typically for a few hours each week) over a several-month period, with on-going experimentation planned to take place for over the entire mission. The measurements readily provide us with information on the growth, the size, and the type of structures formed.

### Hardware Items

The PCS experiment hardware is comprised of an Avionics unit and a Test section unit, each approximately 47 cm x 50 cm x 56 cm in size. The Test Section and Avionics Section are accommodated side by side in ISS EXPRESS Rack 2, occupying four Middeck Locker Equivalents of rack volume (Figure 1). The PCS hardware uses the EXPRESS Rack utilities of power, air-cooling, water-cooling, and communication for commanding and data telemetry. The PCS Avionics Section provides power distribution, command and data communication, data acquisition and processing, and data storage on 18 GB removable hard drives. The PCS Test Section contains eight colloid samples and all the diagnostic instrumentation. A schematic of the PCS science diagnostics is shown (Figure 2). These diagnostics are mostly light scattering instrumentation, which was substantially developed under a previous flight experiment, the Physics of Hard Spheres Experiment (PHaSE).<sup>1,2</sup> Dynamic and Static (D&S)

Light Scattering (aka fiber scattering) is provided via a 532 nanometer Nd-YAG laser and fiber-coupled single photon counting detectors. Two detection fibers simultaneously collect light at scattering angles from 11° to 169° and the complementary angle. Bragg scattering is measured over the range from 10° to 60° by imaging the scattering from a second Nd-YAG laser on an optical screen with a digital camera. Additional optics and a second digital camera capture the laser light scattered at low angles of 0.3° to 6.0°. Via the electronics and data processing provided by the Avionics Section, both static and dynamic light scattering data is obtained from the low scattering angle optics and camera. Static light scattering refers to the measurement of the average angular distribution of the scattered light. This distribution is a measure of the Fourier transform of the mass-to-mass correlations in the sample, meaning that this type of measurement provides information about the sizes or positions of the colloids or structures formed and how they are arranged on length scales up to approximately 5 microns. Dynamic light scattering is a technique that measures the spectral width or time dependence of the scattered light, resulting from the motions of particles or structures. Two color cameras (1x and 10x magnification) provide real-space images on macroscopic length scales (to complement the Fourier-space light scattering on microscopic length scales). A detailed description of the PCS hardware has been previously given by Ansari et al.,<sup>3</sup> while a detailed description of the PCS experiment objectives has been provided by Doherty et al.<sup>4</sup> A detailed description of the hardware operations and command capability is provided by Bowen in the PCS Operations Manual.<sup>5</sup>

### **Operations**

PCS was remotely operated from the NASA Glenn Research Center's (GRC's) Telescience Support Center in Cleveland, Ohio (Figure 3) and at an established remote site at Harvard University in Cambridge, Massachusetts. The two locations permitted daily remote operation of the experiment. All science runs were coordinated with NASA Marshall Space Flight Center's Payload Operations and Integration Center (POIC) for command opportunity and ISS resources. The PCS commanders control such activities as which sample to interrogate, which diagnostic technique to utilize to perform the interrogation (and with what governing execution parameters), as well as the sequencing of sample diagnostic runs. Minimal crew time is required for PCS operations beyond hardware setup and activation, deactivation and removal, and transfer to and from the Space Shuttle. The crew performs data hard drive changeouts as well as

unplanned diagnostic or shutdown procedures as required.

### **Session Table**

These experiments were carried out over 2400 hours of operations. In every session opportunity, many of the diagnostic methods were used to investigate the various samples. These details are summarized in the 'results: completeness /quality of data' section.

## **III. RESULTS**

### **A. List of Pre-, In-, and Post-flight Anomalies**

On Sunday, February 24, 2002, at the onset of a scheduled operational run, the PCS flight system computer failed to boot up. After various intense recovery attempts, including one on Wednesday, March 20, 2002, in which an ISS crew member, Carl Walz, executed a set of uniquely planned, designed, and verified procedures in which he electrically jumper-connected a monitor and keyboard borrowed from the Human Research Facility (HRF) presently on-board ISS, to the PCS flight system computer to access and modify possible corrupted PCS Basic Input/Output System (BIOS) settings, but this recovery operation was without success. In the week following the March 20th recovery attempt, based on several logistics and risk factors, GRC and the ISS program agreed to terminate any further on-orbit recovery actions for the PCS flight hardware.

The hardware was brought down on STS-111 (ISS Flight UF-2) on June 19, 2002 for failure analysis. It was repaired and is ready for the next planned activity with the PCS+ experiments by Profs. Paul Chaikin, and William Russel of Princeton University, and the next PCS-3 experiments by Profs. Dave Weitz, Eric Weeks, and Mike Solomon of Harvard, Emory, and Univ. of Michigan respectively.

Despite the various successes with each and every sample type investigated, PCS was terminated early, and that resulted in some significant missed opportunities. There is one lesson learned. Payload Developers (PDs) would benefit if there was an increase in crew positive reporting. This became evident on March 20, 2002 when the Expedition 4 astronaut executed the PCS troubleshooting procedures. The PCS team would have been more apprised of the status and been able to provide the POIC/ Paycom and OC with real time constructive feedback to better guide the process, if we had been kept informed by a regular set of call downs from ISS.

## B. Completeness/Quality of Data

The total identified science for the experiment was 111%. 81.4% (76.4% baseline science) completeness was achieved in these experiments (See Fig.3.) As the experiments progressed, 11% more science experiments were identified beyond the 100% of the baseline science experiments planned prior to the flight. These are represented by the portions above the 100% line in figure 3. However, the unexpectedly slow growth of one of the samples indicated that 8.125% became impossible to achieve in the time available. Thus, the revised goal was 102.875%. In addition, because of the downtime for the experiment, if the experiment were restored at the next trouble-shooting opportunity in 4/'02, the best possible science completeness would have been 96.88%. Thus,  $(96.875-81.4) = 15.475\%$  became the recoverable science.

The following is a list of missed opportunities in this experiment: The measurements of the growth of the AB6 sample at early times are obscured by scattering from the liquid, and the data we have were not obtained at the optimum time intervals during the growth process; further experiments were planned to investigate this more closely. This would have provided critical insight into the nature of the nucleation and growth process of the crystals, one of the key aspects of the formation of these structures. Similarly, it is essential to repeat the measurements of the early stages of the AB13 crystals to confirm the unexpected power laws observed; this was planned but can not be done. Without these measurements, our results will be incomplete and less convincing to the scientific community.

Likewise, with col-pol gel samples, further experiments were planned to extend the range of frequencies over which the modulus was measured. Rheology measurements as a function of time after the gelation and during the period of aging would have provided valuable insights into the mechanisms leading to structural changes. These results would have provided important additional insight into the nature of the gel.

In the Col-pol critical sample, we needed to repeat the test for confirming certain aspects of the set of data we obtained, and we had hoped to obtain a second "movie" of the spectacular spinodal decomposition behavior in these samples in microgravity, in subsequent experiments.

With the fractal samples, we were not able to probe the aging of the silica gel, and compare the results to that of polystyrene gels; this was one of the main motivations of the experiment. The aging of a gel made from a hard material, silica, should be dramatically different from

that of a soft sample, polystyrene. This conjecture was not tested.

In the case of the glass sample, a new mixing procedure was developed for this sample but there was not sufficient time to fully test it before the apparatus failed.

## C. Tables, Graphs, Figures Index

Table.1 provides the PCS flight samples details and some sample pictures from the space experiments. The details of the close to 2400 hours of experiments are beyond the scope of this document. The operational accomplishment reports and other documents listed in the references and the several upcoming journal publications discuss the results in much further detail.

## D. Photographs:

Not Applicable.

## E. Status of Data Analysis

Analysis of the flight data from this PCS experiment is almost complete. We also completed several post-flight tests on the fluid samples and the test-section and avionics hardware. In addition, we have been conducting additional ground based experiments to help understand the physics that was uncovered by the flight data.

## F. Final Investigation Results

Binary Alloy Colloidal Crystals: We have analyzed all the data to determine the growth rates of the crystals. We find that there is an induction period where no crystals are formed, then a rather rapid growth period where most of the crystals form, and then a very slow coarsening period. We are also conducting confocal microscope studies of the structures formed on earth to gain further insight into this behavior, but we have not yet been successful in making the requisite samples.

Colloid-Polymer Mixture: We have analyzed all the scattering and imaging data to determine the growth of the characteristic length as a function of time. In addition, we have investigated the light scattering and find that the structure factors can be scaled together, and are reasonably well described by theory. The same theory also provides a reasonably good description of the time evolution of the characteristic size. From the data, we are able to determine the surface tension between the two regimes, which drives the coarsening at late times. We find that it is about two orders of magnitude lower than expected, suggesting that we are approaching the critical point of the phase separation. This is certainly the lowest surface tension reported for colloid mixtures. Based on these results, some aspects of these col-pol samples will be tested in the upcoming BCAT-3, PCS-3 and PCS-2 experiments.

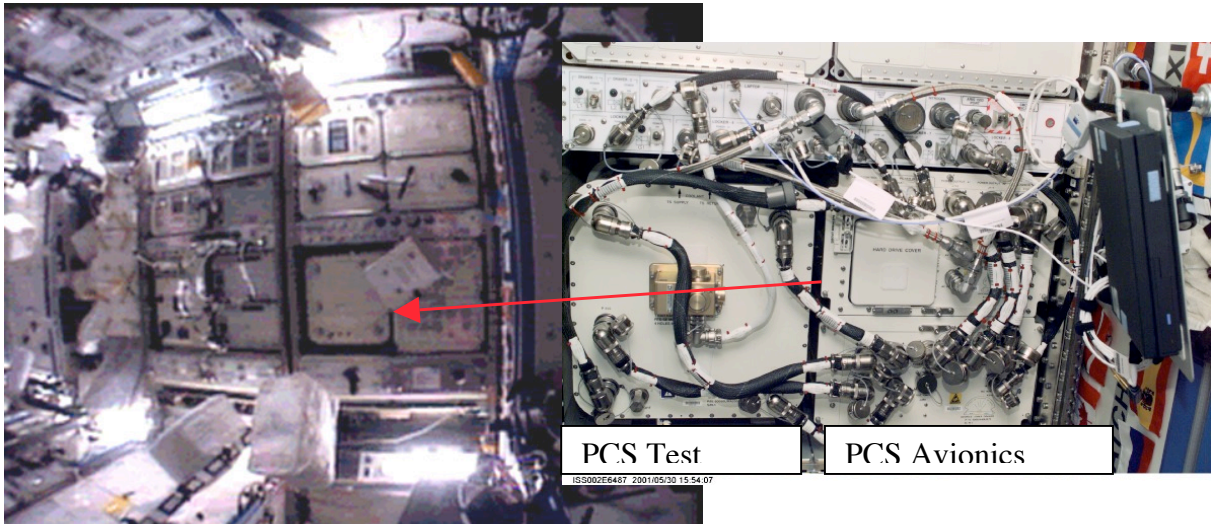


Figure 1 PCS on ISS

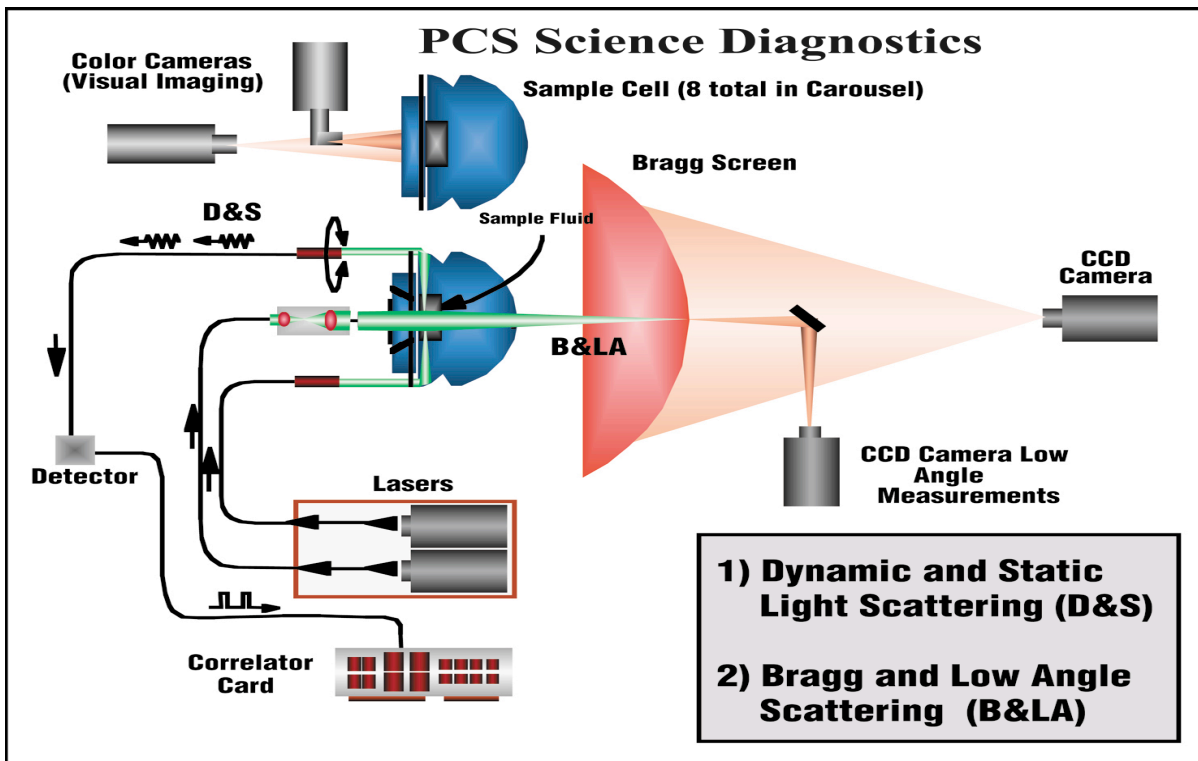
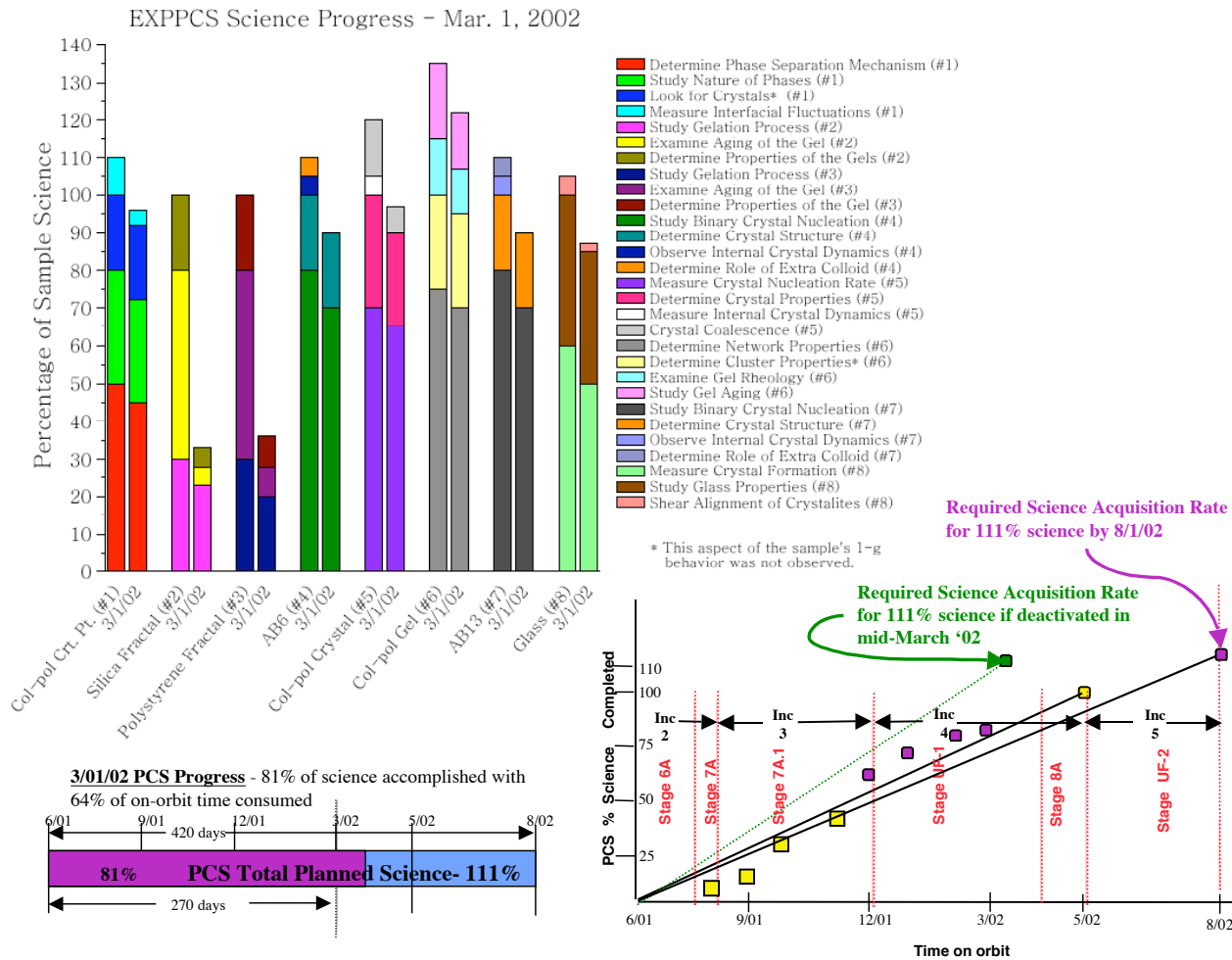


Figure 2 Schematic of the PCS Science Diagnostics



**Fig.3 PCS Final Science Progress**

The bar graph shows the actual science objectives achieved and the total science objectives planned for each of the eight fluid samples. 81% of the total planned science objectives were achieved. Also shown is the rate at which the various science objectives were achieved over the entire experiment duration.

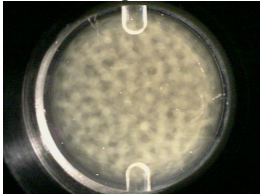
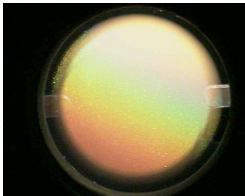
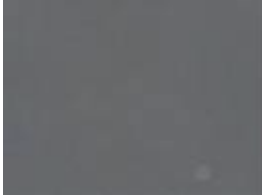
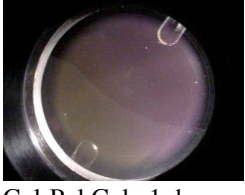
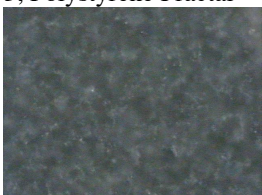
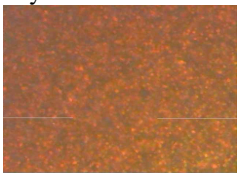
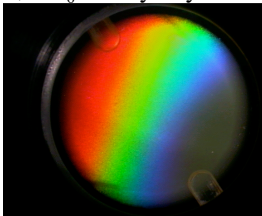
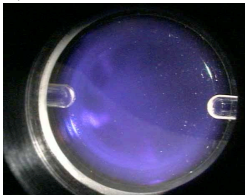
Cell # , Sample Name, sample image	Sample Details	Cell # , Sample Name, sample image	Sample Details
1, Col-Pol Critical Point sample: 11hrs:45mins after mixing. 	r=170 nanometer Colloid and Polystyrene Polymer (Mw=13.2e6); Volume fraction is Colloid: 0.22 Polymer concentration is Cp =1.285 mg/cm <sup>3</sup> Solvent is cis-decalin and tetralin – index match particles; Sample displays strong low angle scattering	5, Col-Pol Crystal 1 hr and 32 minutes after mixing 	r=270 nanometer PMMA Colloid and Polystyrene Polymer; (Mw =3.9e6); Volume fraction Colloid: 0.325 Polymer concentration is Cp =1.055 mg/cm <sup>3</sup> Solvent is cis-decalin and tetralin – index match particles
2, Silica Fractal  Soon after constituent combination.	Silica Ludox TM50 Dupont in water, D=22 nanometers, volume fraction = 1.5e-4, Salt is NaCl (4M)	6, Col-Pol Gel  Col-Pol Gel , 1 day 23 hrs and 40 minutes after mix	ASM8 (r=324.7 nanometer) Colloid and Polystyrene Polymer (Mw =1.98e6, Radius = 38 nanometer, Size ratio is 0.12 (polymer to colloid); Volume fraction is Colloid: 0.25; Polymer concentration is Cp =5.0 mg/cm <sup>3</sup> . Solvent is cis-decalin and tetralin – index match particles. Sample displays a near static scattering ring at low angles.
3, Polystyrene Fractal  Polystyrene Fractal gel: high-mag image 10 days after constituent combination.	Polystyrene (IDC white sulfate 21 nanometer diameter) in water (63% D2O, balance H2O). Volume fraction 8.2e-6; Salt Solution: MgCl <sub>2</sub> (0.1 M) in Water (63% D2O, balance H2O)	7, AB <sub>13</sub> Binary Crystal  AB <sub>13</sub> : High-mag image.	Vol. Fraction of A (r=415nm) is 0.115, and Vol. Fraction of B (r=237.6nm) is 0.41. Radius ratio is 0.5725. Solvent is cis-decalin and tetralin – index match particles. Crystallization time 5 days
4, AB <sub>6</sub> Binary Crystal  Color image of the AB <sub>6</sub> test cell.	Vol. Fraction of A (r=324.7nm) is 0.4167, and Vol. Fraction of B (r=130nm) is 0.1254. Radius ratio is 0.4004. Solvent is cis-decalin and tetralin –index match particles Crystallization time 2 days.	8, Colloidal Glass  Colloidal Glass sample, 2 hrs 33 min after mix.	0.508 micron poly-methyl methacrylate (PMMA) colloid Total volume fraction is : 0.612 Solvent is cis-decalin and tetralin – index match particles Crystallization time: a few days

Table1. PCS Flight Samples Details, and some sample pictures.

**Fractal Colloid Gels:** We have analyzed the polystyrene gel in detail. We are able to completely interpret the correlation functions at all times and all scattering wave vectors,  $q$ . At high  $q$ , the dynamics are dominated by the internal fluctuations, which can be analyzed in terms of a model for fractal gels that we published several years ago. At low  $q$ , the data are best described by diffusional motion of rigid clusters, both translational and rotational. Again, we have developed a theory which describes this. All of the data are well described by these two regimes. We use the low  $q$  data to determine the growth in the cluster size. To account for the polydisperse cluster distribution, and to incorporate the effects of rotational diffusion, we use the fact that the  $q$ -dependent data all scale together, allowing us to extract the average cluster size with no ambiguity. We find that the cluster size continues to increase, just as expected for diffusion-limited cluster aggregation. By contrast, on earth, we find that the size saturates, even for the best buoyancy-matched samples. This saturation occurs at exactly the point predicted by a theory that considers the effects of gravitational drag through the fluid. Thus, this shows that there is a limit to the lower volume fraction that can be gelled on earth. We are also continuing to analyze the data obtained on earth to fully sort out all the effects of gravity on the growth. Finally, we carried out more extensive analysis on the silica gel, and performed some additional supporting experiments on earth. Further detailed results that have been documented to date are available<sup>6-16</sup>.

### G. Conclusion

Physics of Colloids in Space (PCS), the first fluids physics experiment carried out onboard the ISS, has given us tremendous amount of fresh scientific data and knowledge. Four classes of colloids were examined in these experiments, forming binary crystals, col-pol gels and crystals, fractal gels, and glasses. Settling of the particles and aggregates in 1g affects these experiments in various ways; the long durations of microgravity available in the ISS helped unmask these unique data by avoiding such settling, and by extending the experimentation time, thereby allowing us to choose the various samples and study the various growth and coarsening characteristics associated with each.

### H. Earth Benefits / Spin-off Applications

Colloids can be defined as fluids with other particles dispersed in them, particularly particles of size between one nanometer and one micrometer. At the lower bound, the particle sizes are on the order of molecular dimensions, and at the upper bound

external forces such as gravity are more important than Brownian motion.

The variations in sizes, shapes (spheres, rods, etc.), the volume fractions of the particles involved, the surface charge types and distributions, and the properties of the fluid medium, lead to diverse colloidal systems with several technical applications. It is fascinating to see the resulting widespread colloids phenomenon in nature and in industrial processes. Aerosols, foam, paints, pigments, cosmetics, milk, salad dressings, and several electro- and magneto- rheological fluids are examples of colloidal dispersions or suspensions. Abundant biomedical applications for colloidal crystals are being developed; some examples are drug delivery, biomimetic assemblies, cell encapsulation, tissue culture, and controlled release of drugs, flavors, nutrients, and fragrances. Optical, and information and computer technologies can benefit from "colloid engineering" of novel materials such as photonic crystals, via self-assembly in microgravity.

### IV. BIBLIOGRAPHY

1. Lant, C. T., Smart, A. E., Cannell, D. S., Meyer, W.V., and Doherty, M. P., "Physics of hard spheres experiment - a general purpose light scattering instrument," *Appl. Opt.* **36**, 7501-7507 (1997).
2. Doherty, M.P., Lant, C.T., Ling, J.S. "The Physics of Hard Spheres Experiment on MSL-1: Required Measurements and Instrument Performance," AIAA-98-0462 (1998)
3. Ansari, R. R., Hovenac, E. A., Sankaran, S., Koudelka, J. M., Weitz, D. A., Cipelletti, L., and Segre, P.N., "Physics of Colloids in Space Experiment," *Space Technology and Applications International Forum - STAIF-99* (1999).
4. Doherty, M. P., Koudelka, J. M., Motil, S. M., Saavedra, S. M., "Light Scattering for Complex Fluids Research on ISS: Investigator Dreams and Anticipated Hardware Development," AIAA-99-0964 (1999).
5. Bowen, J., "PCS Operations Manual," PCS-DOC-050, unpublished (2001).
6. Weitz, D.A, Bailey, A., Manley, S., Prasad, V., Christianson, R., Sankaran, S., Doherty, M., Jankovsky, A., Lorik, T., Shiley, W., Bowen, J., Kurta, C., Eggers, J., Gasser, U., Segre, P., Cipelletti, L., Schofield A., and Pusey, P., "Results from the Physics of Colloids Experiment on ISS," *World Space Conference, 53rd Int. Astronautical Congress Houston, TX, '02 IAC-02-J.6.04. & NASA/ TM-2002-212011, Dec. '02.* <http://gltrs.grc.nasa.gov/cgi-bin/GLTRS/browse.pl?2002/TM-2002-212011.html>

7. Weitz, D.A, et al., "Physics of Colloids in Space," 6th Microgravity Conference, Cleveland, OH, 2002. Plenary Lecture.
  8. Christianson, R, Weitz, D.A., et al., "Binary Colloidal Crystals," 6th Microgravity Conference, 2002. Poster. (abstract/ poster presentation.)
  9. Doherty, M., Sankaran, S., et al., "PCS: The First Fluid Physics Payload on ISS", Proceedings of the Sixth Microgravity Fluid Physics & Transport Phenomena Conference, <http://gltrs.grc.nasa.gov/reports/2002/CP-2002-211212-VOL2/>, pp. 5-7, August, 2002, (abstract/ poster presentation.)
  10. Weitz, D.A, et al., "Early Results from ISS Experiments," ISS Utilization conference, Florida, 2001 Plenary Lecture.
  11. Doherty, M., and Sankaran, S., Physics of Colloids in Space (PCS): Microgravity Experiment Completes Operations on ISS", NASA R&T 2002 Report Article, 2003, pp. 224-226, [www.grc.nasa.gov/WWW/RT](http://www.grc.nasa.gov/WWW/RT)
  12. Doherty, M., and Sankaran, S., Physics of Colloids in Space (PCS): Microgravity Experiment Launched, Installed, and Activated on the ISS", NASA R&T 2001 Report, p.195-197, NASA/TM-2002-211333, 2002, [www.grc.nasa.gov/WWW/RT](http://www.grc.nasa.gov/WWW/RT)
  13. Weitz, D.A., Pusey, P., Bailey, A., Sankaran, S., and Doherty, M.P., "ISS Increment 4 Operational Accomplishments Report -- Physics of Colloids in Space (PCS)," Aug. 2002, ISS Research Program Postflight Reports, (cd), Vol .2, 2003.
  14. Weitz, D.A., Pusey, P., Bailey, A., Sankaran, S., and Doherty, M.P., "ISS Increment 3 Operational Accomplishments Report -- Physics of Colloids in Space (PCS)," March 2002, ISS Research Program Postflight Reports, (cd), Volume 1, 2002.
  15. Weitz, D.A., Pusey, P., Bailey, A., and Doherty, M.P., ISS Increment 2 Operational Accomplishments Report -- Physics of Colloids in Space (PCS), ISS Research Program Postflight Reports, 2001.
  16. Weitz, D.A., website: "The Physics of Colloids in Space (PCS) project", <http://www.deas.harvard.edu/projects/weitzlab/research/nasaproj.html>
-